1-1-2018

Relationship Between TDP-43 Toxicity and Aggregation in Saccharomyces Cerevisiae

Martin Anthony Aguilar
University of Denver

Relationship Between TDP-43 Toxicity and Aggregation in Saccharomyces Cerevisiae

Abstract

Protein aggregation and inclusion body formation are hallmarks of neurodegenerative diseases such as Alzheimer's, Parkinson's, Huntington's, and amyotrophic lateral sclerosis (ALS). These neurodegenerative diseases share a common pathology in that all include accumulation of insoluble protein aggregates in the brain. TAR-DNA-binding protein (TDP-43) is the major component found in the pathological inclusions of two of these diseases, ALS and frontotemporal lobar degeneration with ubiquitin-positive inclusions (FTLD-U). This thesis focuses upon the biophysical basis for TDP-43 aggregation in *S. cerevisiae*. Current *in vitro* evidence indicates that TDP-43 is a natively dimeric protein and that binding to RNA inhibits aggregation. Corresponding genetic results in yeast in which specific components of the RNA-decay machinery have been knocked-out, indicate that the buildup of specific cellular RNAs is capable of counteracting TDP-43 aggregation and toxicity *in vivo*. This thesis provides evidence of separate pathologies of TDP-43 and TDP-43 mutants in *S. Cerevisiae*. This thesis also introduces preliminary data of the effect of *in vitro* synthesized RNA on TDP-43 toxicity.

Document Type

Thesis

Degree Name

M.S.

Department

Chemistry and Biochemistry

First Advisor

Erich G. Chapman, Ph.D.

Keywords

Amyotrophic lateral sclerosis, Protein aggregation, TDP-43, TAR-DNA-binding protein

Subject Categories

Biochemistry, Biophysics, and Structural Biology | Neuroscience and Neurobiology

Relationship Between TDP-43 Toxicity and Aggregation In Saccharomyces cerevisiae

---

A Thesis

Presented to

the Faculty of Natural Sciences and Mathematics

University of Denver

In Partial Fulfillment

of the Requirements for the Degree

Master of Science

By

Martin A. Aguilar

November 2018

Advisor: Erich G. Chapman

Author: Martin A. Aguilar
Title: Relationship Between TDP-43 Toxicity and Aggregation in Saccharomyces cerevisiae
Advisor: Erich G. Chapman
Degree Date: November 2018

Abstract

Protein aggregation and inclusion body formation are hallmarks of neurodegenerative diseases such as Alzheimer's, Parkinson's, Huntington's, and amyotrophic lateral sclerosis (ALS). These neurodegenerative diseases share a common pathology in that all include accumulation of insoluble protein aggregates in the brain. TAR-DNA-binding protein (TDP-43) is the major component found in the pathological inclusions of two of these diseases, ALS and frontotemporal lobar degeneration with ubiquitin-positive inclusions (FTLD-U). This thesis focuses upon the biophysical basis for TDP-43 aggregation in *S. cerevisiae*. Current *in vitro* evidence indicates that TDP-43 is a natively dimeric protein and that binding to RNA inhibits aggregation. Corresponding genetic results in yeast in which specific components of the RNA-decay machinery have been knocked-out, indicate that the buildup of specific cellular RNAs is capable of counteracting TDP-43 aggregation and toxicity *in vivo*. This thesis provides evidence of separate pathologies of TDP-43 and TDP-43 mutants in *S. Cerevisiae*. This thesis also introduces preliminary data of the effect of *in vitro* synthesized RNA on TDP-43 toxicity.

Acknowledgements

My deepest thank you goes to my family for their love, support, and guidance throughout every stage of my life. I owe an incredible amount of gratitude for the support they've offered me. I also appreciate the love, support, and push given to me from Nicole Savage. She consistently goes above and beyond to guarantee I have the drive and ability to accomplish my goals.

Table of Contents

List of Figures

Chapter One: Introduction

1.1 Overview: Protein Localization in Disease

Eukaryotic cells contain organelles and a complex endomembrane system. These organelles provide distinct compartments for different metabolic activities. Protein translation occurs solely in the cytosol compartment of the cell. Cells require translocation of proteins to exert protein function in different organelles. Approximately half of the proteins generated by a cell are transported into or across one or more cellular membranes to reach their functional location (Chacinska et al. 2009).

Subcellular localization is essential to protein function. Using distinct compartments provides a way to achieve functional diversity and save on protein design and synthesis (Butler and Overall, 2009). Aggregation of amyloidogenic proteins can result in the sequestration, inactivation, and irregular localization of numerous proteins. Aberrantly localized proteins have been linked to human diseases as diverse as amyotrophic lateral sclerosis, cancer, and Swyer syndrome (Winton et al., 2008; Dansen and Burgering, 2008; McLane and Corbett, 2009). In patients with ALS, affected neurons exhibit a prominent redistribution and nuclear inclusions of TAR DNA-binding protein (TARDBP, also known as TDP43) or the protein fused in sarcoma (FUS) from the nucleus to the cytoplasm (Neumann et al., 2006).

1.1.1 Amyotrophic Lateral Sclerosis

Amyotrophic Lateral Sclerosis (ALS) is a late-onset neurodegenerative disease. Characterization of the disease includes loss of motor neurons, progressive weakness, and eventual paralysis leading to death by respiratory failure or pneumonia (Kierman et al., 2011). ALS disease progression results in death within 3-5 years of diagnosis (Boillée et al., 2006). Most ALS cases are sporadic, but 10% are familial. Approxamately 20% of familial cases result from mutations in the SOD1 gene (encoding Cu/Zn superoxide dismutase) and 34% from hexanucleotide repeat expansions in the chromosome 9 open reading frame 72 gene (*C9ORF72*) repeats (Rosen et al., 1993; Blitterswijk et al., 2012). SOD1 mutations are thought to cause disease by a toxic gain of function (Bruijn et al., 1998), thus strategies to lower SOD1 levels are being pursued (Smith et al., 2006). However, SOD1 mutations and *C9ORF72* repeats account for only a small percentage of ALS cases, and additional therapeutic strategies are needed. RNA-binding proteins and RNA-processing pathways have recently been implicated in ALS and may provide another possible therapeutic target (Lagier-Tourenne et al., 2010; Gitler et al. 2011).

1.1.2 TDP-43 aggregation in ALS

TDP-43 was identified as a major component of the ubiquitinated neuronal cytoplasmic inclusions deposited in cortical neurons in FTD and in spinal motor neurons in ALS (Neumann et al, 2006). TDP-43-positive inclusions have subsequently been shown to be common in 97 % of ALS cases (Mackenzie, et al. 2007, Maekawa et al., 2009), whether sporadic or familial. Additionally, mutations in the gene TARDBP,

which encodes TDP-43, have been identified in familial ALS and sporadic ALS cases (Pesiridis et al., 2009; Rutherford et al., 2008; Sreedharan et al., 2008; Van Deerlin et al., 2008; Yokoseki et al., 2008). Therefore, therapies targeting TDP-43 could be effective in cases not caused by SOD1 mutation. Notably, TDP-43 inclusions occur in many frontotemporal dementia cases. Targeting TDP-43 might be an effective therapeutic strategy for these patients. Efforts are under way to define the mechanisms by which TDP-43 and defects in RNA processing pathways contribute to ALS.

The exact cellular function of TDP-43 is officially unknown though experiments show the protein plays a very important role in several biological systems. These systems either regard the control of gene transcription, selected splicing processes, and in the maintenance of mRNA stability.

Gene expression of HIV-1 is regulated by many host cellular factors. TDP-43 was found to inhibit the assembly of transcriptional factors in the regulatory system (Ou et al., 1995). The binding site of TDP-43 was determined using band shift analysis. This sequence was found to be the HIV-1 long terminal repeat known as TAR. The binding section extends from nucleotide -18 to +80 and is important for the activation of gene expression.

The mechanism of TDP-43 toxicity in ALS isn't fully understood. Numerous models exist. One model suggests TDP-43 undergoes nuclear export during times of cellular stress. TDP-43 then moves to a stress granule or undergoes liquid-liquid phase separation. Glycine rich C-terminal domain drives aggregation of TDP-43 causing

sequestering of vital RNAs and other RNA binding proteins (Figure 1). Various studies have examined the roles of TDP-43's gain or loss of function in disease. Overexpression of wild-type TDP-43 recapitulates TDP-43 proteinopathy and disease phenotypes in an array of animal models (Johnson et al., 2008; Wils et al., 2010; Li et al., 2010; Ash et al., 2010). These results support a role for gain of toxic function in disease. Initial studies testing a loss-of-function hypothesis used knock-out of TDP-43 from mice. The complete knock-out of TDP-43 resulted in embryonic lethality (Wu et al., 2010; Sephton et al., 2010; Kraemer et al., 2010). These early studies demonstrated TDP-43 plays a vital role in early development without necessarily demonstrating that loss of function could be degenerative in adulthood. To address these questions, conditional and partial knockout models demonstrated loss of TDP-43 function can induce motor neuron defects, a progressive motor phenotype reminiscent of human disease, and even typical TDP-43 proteinopathy (Wu et al., 2012; Iguchi et al., 2013; Kabashi et al., 2010). Interestingly, either overexpression or knockdown of TDP-43 selectively in glia or muscle also recapitulates ALS-like phenotypes (Yang et al., 2014; Diaper et al., 2013). The emerging picture is that both gain and loss of TDP-43 function may be mechanistic in disease and TDP-43 misfolding may link the two.

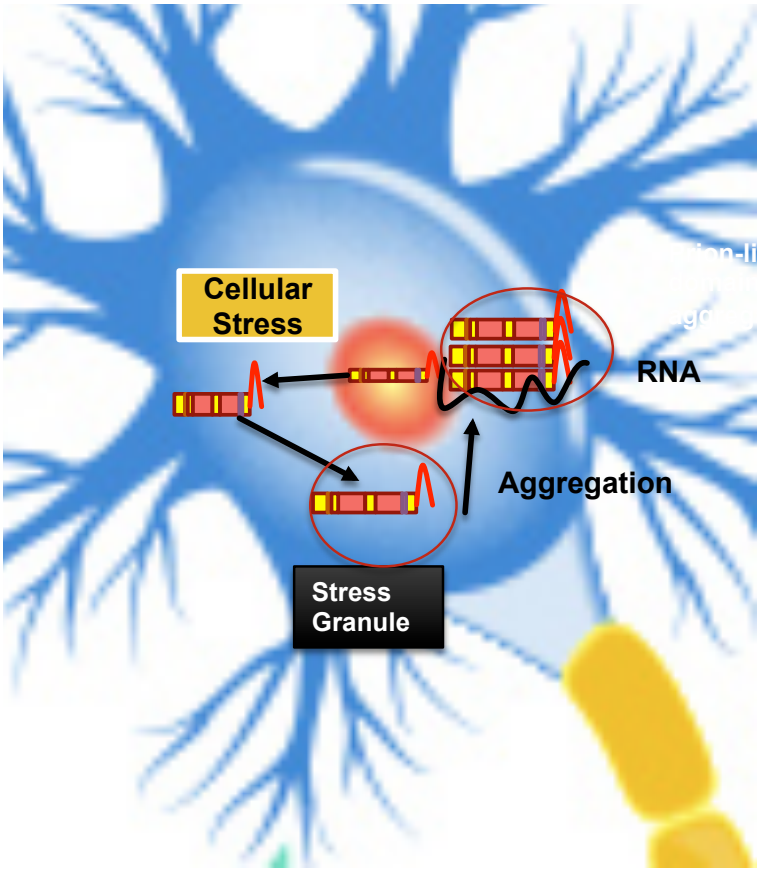

Figure 1: Proposed model of aggregation in yeast. Cellular stress causes nuclear export of TDP-43. TDP-43 moves into stress granule. Glycine rich C-terminal domain drives aggregation of TDP-43 causing sequestering of vital RNAs and other RNA binding proteins.

1.2 TDP-43

Human TDP-43 was first isolated in 1995. The discovery was made while searching for novel transcriptional inactivators that bind the TAR DNA element of the human immunodeficiency virus type 1 (HIV-1) virus. TDP-43 is a ubiquitously expressed and highly conserved metazoan nuclear protein (Ayala et al., 2005). TDP-43

contains two RNA recognition motifs (RRMs) and a glycine-rich C-terminal domain. TDP-43's function is uncertain, but it likely plays important roles in pre-mRNA splicing and transcriptional repression (Ayala et al., 2008; Buratti et al., 2001). The gene coding for this protein (TARDBP) is present on Chromosome 1 and consists of 6 exons. Some of these exons may be alternatively spliced to yield various isoforms of the protein (Wang et al., 2004). TARDBP is a highly conserved gene throughout evolution and relating homologues of human TDP-43 have been found in all higher eukaryotic species. Homologues of TDP-43 were found in distant organisms such as *Drosophila melanogaster, Xenopus laevis, and Caenorhabditis elegans* (Wang et al., 2004; Ayala et al., 2005). Such a high degree of sequence conservation hints towards a fundamental role played by this protein.

In ALS and frontotemporal lobar degeneration with ubiquitin-positive inclusions (FTLD-U), TDP-43 is depleted from the nucleus and accumulates in ubiquitinated cytoplasmic inclusions (Neumann et al., 2006). Notably, mutations in the TDP-43 gene (TARDBP) are linked to sporadic and non-SOD1 familial ALS. This implies that TDP-43 abnormalities are likely one cause of the disease (Kabashi et al., 2008; Sreedharan et al., 2008; Van Deerlin et al., 2008; Rutherford et al., 2008; Gitcho et al., 2008; Yokoseki et al., 2008).

1.2.1 TDP-43 Structure

Full open reading frame of TARDBP consists of 1,245 base pairs coding for 414 amino acids. The theoretical molecular weight of TDP-43 is 44,740 Daltons. TDP-43

contains two highly conserved RNA Recognition Motifs (RRM1 and RRM2) flanked by an N-terminal and a C-terminal tail (Figure 2). This primary amino acid structure resembles that of members of the heterogeneous ribonucleoprotein (hnRNP) family (Krecic et al., 1999; Dreyfuss et al., 2002). The c-terminal tail contains a glycine-rich region often found in proteins to mediate protein-protein interactions.

TDP-43 was found to natively dimerize in normal cells under physiological conditions (Shilina et al., 2010). Formation of a monomer results in a more aggregation prone protein.

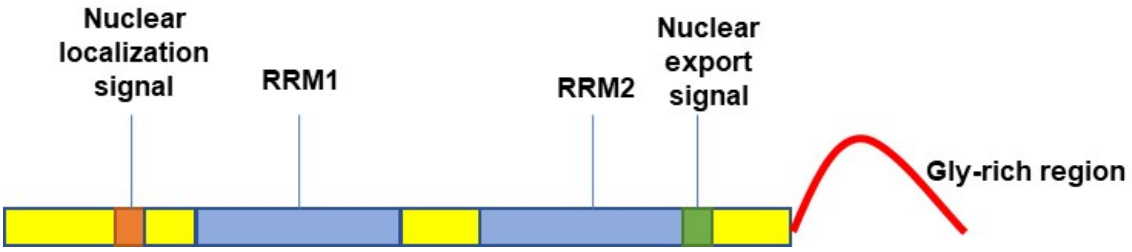

Figure 2: Domain structure of TDP-43. Protein contains a N-terminal domain, two RNA binding motifs, and a "prion-like" unstructured C-terminal domain.

1.2.2 TDP-43 Functions

Eukaryotic gene expression requires the coupling of many processes. These processes include transcription, pre-mRNA processing, mRNA transport, and translation (Maniatis et al, 2002; Proudfoot et al., 2002). Proteins that take part in these processes are not confined to singular roles. The functions performed by TDP-43 seem to be decided by the sequence specificity of the RRM domains. Previous research demonstrated TDP-43 binds single stranded TG and UG repeats with high affinity via the RRM1 domains (Ayala et al., 2005; Buratti et al., 2001). At least 5 repeated units (UG_5)

are necessary for efficient binding of TDP-43 and efficiency increases with increased length (Ayala et al., 2005).

Much less is known about the function of the N-terminal domain. The N-terminal domain is loosely conserved compared to the RRM domains. The length of the N-terminal region varies in different species. The average of most species is 105 residues compared to 174 residues in *C. elegans*. Contrary to the lack of conservation in length, a striking example of conserved sequence exists in a 15-nucleotide region highly enriched in acidic amino acids near the N-terminus of TDP-43 (Buratti et al., 2001).

1.2.3 TDP-43 is Intrinsically Aggregation Prone

In the absence of other components, TDP-43 spontaneously forms aggregates bearing ultrastructural similarities to TDP-43 deposits in degenerating neurons of ALS FTLD-U patients (Johnson et al., 2009). The C-terminal of TDP-43 was also found to be important for aggregation. Truncation of the C-terminal led to a loss of toxicity and aggregation (Johnson et al., 2009). Of the over 25 recently reported ALS- linked TDP-43 mutations, all but one mutation can be found within this domain (Banks et al., 2008). Furthermore, similar aggregated C-terminal fragments accumulate in ALS and FTLD-U (Neumann et al., 2006).

1.2.4 TDP-43 Liquid-Liquid Phase Separation

Stress granules are membrane-less assemblies generated by the condensation of protein and nucleic acid components into liquid phases that self-segregate in the cell. Like other ALS-associated RNA-binding proteins, TDP-43 has been shown to undergo

liquid-liquid phase separation (LLPS) (Molliex et al., 2015). The N and C-termini of TDP-43 can drive the phase separation (Schmidt et al., 2016). Three tryptophan residues (Trp-334, Trp-385, and Trp-412) are the most important residues for TDP-43 LLPS. These results also suggest that only a few residues might be required for TDP-43 LLPS due the self-assembling tendency of the α-helical segment in the middle part of the C-terminal. This reduces the number of motifs required for formation of multiple binding sites (Li et al., 2018). Furthermore, there's evidence that disruption of LLPS increases the pathological fibrilization of these ALS-associated RNA-binding proteins (Taylor et al., 2017).

1.2.5 Mutations of TDP-43

Numerous mutations of TDP-43 have been found in patients with ALS. Testing of these mutations *in vivo* and *in vitro* has yielded various results. ALS-associated TDP-43 inclusions are primarily fragments. These fragments often include the entire CTD (Neumann et al., 2006). The CTD is classified as "prion-like" due to a resemblance to the amino acid frequency in yeast prion domains. This includes a low complexity composition rich in polar while also and poor in aliphatic and charged residues (King et al., 2012). The domain proves to be aggregation-prone in both *in vitro* and *in vivo* models of ALS (Budini et al., 2015; Johnson et al., 2009; Wegorzewska et al., 2009). Additionally, mutations in the CTD can have a profound effect on the behavior of the domain. TDP-43 C-terminal domain liquid-liquid phase separation is mediated by intermolecular interactions that include contacts involving the 321-340 region. ALS

mutations (A321G, Q331K, and M337V) significantly disrupt phase separation stimulating the conversion to aggregates. Some of these mutations result in a disruption of the helical structure (possibly leading to an increase in aggregation) (Conicella et al., 2016).

Native dimerization of TDP-43 occurs via the N-terminal domain interface. This interface mainly occurs by way of hydrogen bonding and electrostatic forces between the N-terminal domain and RRM domains of two TDP-43s. Mutation of serine to glutamic acid at the 48th residue disrupts hydrogen bonding in the interface and weakens the assembly of the dimeric state by removing the hydrogen bonding and electrostatic interaction capabilities (Wang et al., 2018).

Mutations in the RRM1 have also been assessed. Mutating phenylalanine 147 and phyenylalanine 149 to leucines result in the inability of TDP-43 to bind RNA or DNA (Buratti et al., 2001). TDP-43 can no longer bind DNA or RNA due to the loss of pi-pi stacking interactions in the domain.

1.2.6 Enhancing TDP-43 Solubility Via RNA Binding

TDP-43 is a 414-amino acid nuclear protein composed of two highly conserved RNA recognition motifs (RRM1 and RRM2) and a glycine rich C-terminal region. Both RRMs are involved in binding of RNA/ DNA sequences enriched in UG or TG repeats. Recent findings also suggest that RNA/DNA binding modulates TDP-43 solubility (Pesiridis et al., 2011; Huang et al., 2013). These studies have shown that poly-TG compounds can increase the solubility of refolded recombinant TDP-43 under

aggregation conditions induced by temperature (Huang et al., 2013). These experiments provided evidence that inhibition of aggregation occurs by preservation of the protein's native dimeric state and prevention of a monomeric state. Additionally, poly-TG compounds increase the solubility of TDP-43 greater than naturally occurring nucleotide targets (Sun et al., 2014). Length of TG/UG repeats and molar concentration of the repeats also had an inverse relationship with Kd values (Bhardwai et al., 2013). These discoveries provide a possible method of preventing TDP-43 aggregation using DNA or RNA therapies. Increaseing the stability of RNAs in the cytoplasm may also play a role in therapy effectiveness.

1.3 mRNA Structural Stability

Recent studies have revealed that long non-coding RNA (lncRNA) stability varies widely (<0.5 h to >48 h). These findings hint at transcript half-life being one factor that regulates biological function (Clark et al., 2012; Tani et al., 2012). Messenger RNA (mRNA) degradation rates change in response to stimulus. This allows cells to quickly increase or decrease mRNA abundance to meet a cell's needs for specific proteins. Collections of bound proteins and noncoding RNAs dictate mRNA degradation rates through their ability to recruit (or exclude) the mRNA degradation machinery. Deadenylation dependent mRNA decay is the major pathway in mammalian cells. One or a combination of three deadenylases performs poly(A) tail removal. These particular enzymes utilized appear to be mRNA specific (Garneau et al., 2007; Goldstrohm and Wickens, 2008).

Following deadenylation, degradation of a mRNA continues in a 5′ to 3′ or 3′ to 5′ direction. 3′ to 5′ decay of the mRNA body requires the 10 to 12 subunit exosome. This contains RNase PH-domain enzymes, S1 and KH-family RNA-binding proteins, RNase D-like enzymes, and RNA helicases (Mukherjee et al., 2002; Houseley et al., 2006). When only a few 5′ nucleotides of the mRNA remain, the decapping enzyme DcpS removes the 5' cap structure (Liu et al., 2002). 5′ to 3′ mRNA decay begins with decapping. Dcp1 and Dcp2 proteins come together to perform the decapping. Decapping requires several other proteins including Lsm1–7 (bound at the 3′- end of the deadenylated product), hEdc3, Rck/p54, and Hedls. Hedls enhances the decapping activity of Dcp2 and promotes complex formation between Dcp1-Dcp2 (FengerGron et al., 2005). Xrn1 degrades the mRNA following decapping.

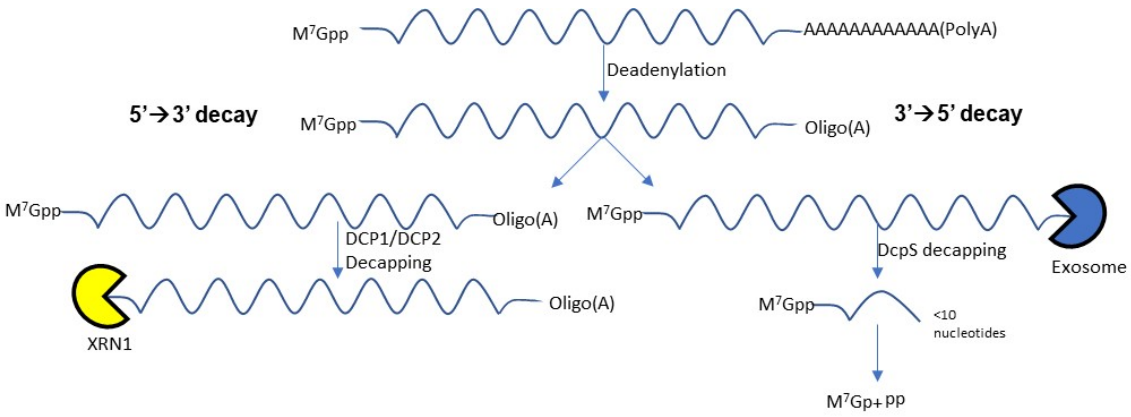

Figure 3: Representations of 5' and 3' mRNA decay. Deadenylation One or a combination of three deadenylases performs poly(A) tail removal. Following deadenylation, degradation of a mRNA continues in a 5′ to 3′ or 3′ to 5′ direction. 5' to 3' decay proceeds with 5' decapping by DCP1 and DCP2 followed by decay via XRN1. 3' to 5' decay proceeds with decay using a 3' exosome until only a few nucleotides remain. 5' decapping then occurs via DcpS.

1.3.1 XRN1-resistant RNA (xrRNA)

Flaviviruses are single-stranded positive-sense RNA viruses (Bhatt et al., 2013; Mackenzie et al., 2004; Normile et al., 2013). The flavivirus genus includes, but is not limited to, West Nile Virus, dengue virus, yellow fever virus, and Zika virus (Chambers et al., 1990). Most of these viruses are transmitted by bite from an infected mosquito or tick. During infection, not only is the viral genomic RNA (gRNA) replicated, but specific 300–500 nucleotide-long subgenomic flaviviral RNAs (sfRNAs) also accumulate from the incomplete degradation of the 3' untranslated region (3'UTR) (Pijlman et al., 2008). This incomplete degradation is performed by the 5'to 3' host-cell exonuclease Xrn1 (Jones et al., 2012). sfRNAs form from a halt in degradation at defined locations within the gRNA's 3'UTR (Pijlman et al., 2008).

Sequence alignment of xrRNA suggests a shared structure. Helices P1 and P2 of the RNA stack coaxially while helix P3 is at an acute angle relative to P1 (Chapman et al., 2014). This structure is consistent with other RNA three-way junctions from flaviviruses (Lescoute et al., 2006). Together, helices P1 and P3 form a ring-like structure. The continuous loop comprised of Nucleotides 33-49 resides entirely on one side of the structure. The 5'end of the xrRNA passes through the center of the ring. Xrn1 encounters the compact and concave ring-like side of the xrRNA as it degrades the RNA in a 5' to 3' direction (Chapman et al., 2014).

Upon encountering the concave ring-like structure, Xrn1 must pull the 5' end of the RNA through the ring. Unfolding this xrRNA requires Xrn1 to essentially turn the

structure inside out. During strand synthesis, the virally encoded RNA polymerase would not encounter this impediment as it approachs from the 3' end. This suggests the characteristic of unidirectional resistance (Chapman et al., 2014).

1.3.2 3' Expression and Nuclear Retention Element (ENE)

Metastasis-associated lung adenocarcinoma transcript 1 (MALAT1) is a highly abundant, nuclear-localized lncRNA. MALAT1 is also a precurser for the tRNA-like structures known as mascRNA. The structures are substrates for RNase P (Hutchinson et al., 2007; Bernard et al., 2010; Stadler, 2010; Wilusz et al., 2008; Sunwoo et al., 2009). The resulting 5′-cleavage products of MALAT1 end with a highly conserved sequence. This sequence contains two U-rich motifs and a genomically encoded A-rich tract at the 3′ end (Wilusz et al., 2008; Sunwoo et al., 2009). *In vitro* decay assays have shown a destabilization effect from mutations in the U-rich motifs and A-rich tract in mouse MALAT1 RNA fragment. This result suggests the structure of this region contributes to RNA stability despite the lack of a traditional poly(A) tail (Wilusz et al., 2008; Guhaniyogi et al., 2001). This structure has U•A-U base triples flanked by two stems. The 3′ sides of the U-rich internal loops can form 11 consecutive Watson–Crick base pairs with the downstream A-rich tract, and the 5′ sides are proposed to engage in Hoogsteen interactions. Analyses of the MALAT1 ENE revealed that stabilization activity requires an intact triple helix, strong stems at the duplex-triplex junctions, a G-C base pair flanking the triplex to mediate potential A-minor interactions, and the 3′-

terminal A of the A-rich tract to form a blunt-ended triplex lacking unpaired nucleotides at the duplex- triplex junction (Brown et al., 2012)

1.4 Saccharomyces cerevisiae Genomics

The budding yeast*, Saccharomyces cerevisiae* (*S. cerevisiae*), serves as an important experimental organism for revealing gene function. In addition to carrying out all the basic functions of eukaryotic cells, up to 30% of positionally-cloned genes implicated in human disease have yeast homologs (Bassett et al., 1997). *S. Cerevisiae* are also utilized because of the ease with which it can be manipulated. For these reasons, *S. cerevisiae* research serves as a model organism for a variety of processes that occur in humans.

The Gateway® cloning method for use in *S. cerevisiae* was developed to address the time-consuming nature of standard cloning methods. The system adapted the pRS series of yeast shuttle vectors. These vectors are based on the site-specific recombination properties of the bacteriophage lambda (Landy, 1989). The lambda recombination system requires two major components: DNA recombination sites and enzymes to facilitate the recombination reaction. A mixture of enzymes that bind to specific sequences catalyzes the recombination. The enzymes bring together the target sites, cleave them, and covalently attach the DNA. Recombination occurs following two pairs of strand exchanges and ligation of the DNAs in a novel form. The recombination proteins involved in the reaction differ depending upon whether lambda utilizes the lytic or lysogenic pathway. The lysogenic pathway is catalyzed by the bacteriophage λ

Integrase (Int) and E. coli Integration Host Factor (IHF) proteins (BP Clonase™ enzyme mix). The bacteriophage λ Int and Excisionase (Xis) proteins, and the *E. coli* Integration Host Factor (IHF) protein catalyze the lytic pathway (LR Closest enzyme mix) (Landy, 1989; Ptashne, 1992).

Pathway	Reaction	Enzymes
Lysogenic	attB x attP→attL x attR	BP Clonase (Int, IHF)
Lytic	attL x attR→attB x attP	LR Clonase (Int, Xis, IHF)

Figure 4: Gateway Clonase reactions: BP reactions follow the Lysogenic pathway. LR reactions follow the Lyctic pathway. Each pathway uses a unique set of enzymes to accomplish the recombination reaction.

ORFs are first moved from a PCR product or entry clone to a donor vector. At this stage, ORFs are flanked by attB sites. The attB sites on the ORF react with the attP sites on a donor vector. This BP reaction results in the ORF in a donor vector with attL sites. The new donor vector is then moved from the donor vector to a destination vector. This stage utilizes the attL sites on the donor vector and attR sites on the destination vector. This LR reaction results in the ORF in a destination vector with attB sites.

288 yeast Gateway® vectors were developed using two commonly used GPD and GAL1 promoter expression systems. Using these systems enable expression of ORFs either constitutively or under galactose-inducible conditions. The expression system also enables proteins of interest to be fused to a choice of frequently used N- or C-terminal tags. These tags include EGFP, ECFP, EYFP, Cerulean, monomeric DsRed, HA or TAP.

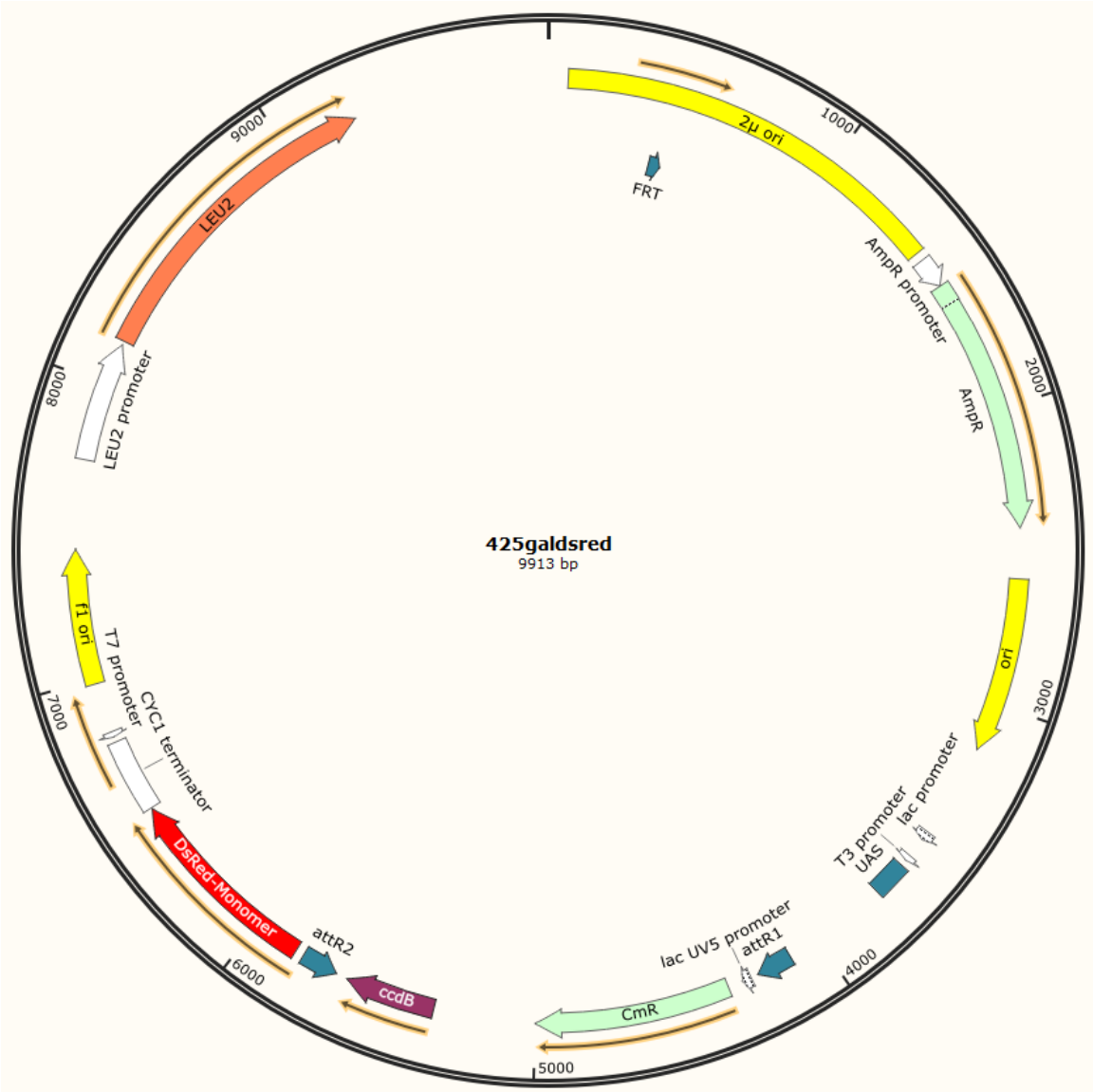

Figure 5: Gateway Destination Vector. 2µ ori: fragment from the 2 micron circle (a natural yeast plasmid) allows for 50+ copies to stably propogate per cell.. AmpR: coding sequence gives E coli containing the plasmid ampicillan resistance. attR1 and attR2 sites for site specific recombination. ccdB gene: bacterial toxin that poisons DNA gyrase for selection of successful LR products. DsRed Monomer: C-terminal DsRed fluorescent tag.

1.4.1 Using Yeast as a TDP-43 Proteinopathy Model

TDP-43 toxicity and aggregation were reported using yeast (Johnson et al., 2008). This model recapitulates numerous distinctive cellular features of human TDP-43 pathology, including conversion from nuclear localization to cytoplasmic aggregation. The pathological features of TDP-43 are distinct from those of other protein-misfolding diseases in yeast models (Johnson et al., 2008). This suggests that rather than general cellular stresses associated with accumulating misfolded proteins, the yeast model reveals specific aspects of the underlying biology of the disease associated with TDP-43 aggregation. This work provided framework for investigating the toxicity of TDP-43 aggregation relevant to human disease while also establishing a manipulable model for discovering potential therapeutic strategies (Johnson et al., 2008).

The manipulability of yeast provided the ability to perform a genome-wide screen to identify genes that modify TDP-43 toxicity (Giaever et al., 2002). Deletion of the lariot debranching enzyme (*dbr1)* provided the most potent suppressor of TDP-43 toxicity (Armakola et al., 2012). *dbr1* catalyzes the debranching of lariat introns that are formed during pre-mRNA splicing. In yeast, it was shown that inhibiting the debranching enzymatic activity of *dbr1* sufficiently rescued TDP-43 toxicity (Armakola et al., 2012). Evidence was also provided that intronic lariat species that accumulate in the cytoplasm of *dbr1*Δ cells act as decoys to sequester toxic cytoplasmic TDP-43 (Armakola et al., 2012). This possibly prevents aggregated TDP-43 from interfering with other essential cellular RNA targets and RNA-binding proteins. Knockdown of *dbr1* in a

human neuronal cell line and in primary rat neurons is also sufficient to rescue TDP-43 toxicity, suggesting that the effect of *dbr1* on TDP-43 toxicity is conserved from yeast to mammals (Armakola et al., 2012).

1.5 RNA Aptamers

Nucleic acids were once only considered as the key molecules solely involved in storage and expression of genetic information. That narrow outlook changed after the discovery of non-coding RNAs. These RNAs exploit the structural characteristics of nucleic acids to execute a variety of functions. These functions include gene regulation, catalysis, and specific ligand binding (McKeague et al., 2012). Following this discovery, a new class of synthetic nucleic acid molecules called "Aptamers" developed. These are small single stranded DNAs or RNAs. These DNAs and RNAs range from 15 to 150 nucleotides with an ideal length of 20-40 nucleotides (Wang et al., 2012). These DNAs and RNAs fold into a well-defined three–dimensional structure. These structures allow binding to target ligands with high affinity and specificity (Mayer, 2009; Tuerk et al., 1990).

1.5.1 MS2 System

Aptamers have been developed to visualize RNA *in vivo*. In 1998, a method was introduced to visualize mRNA dynamics in live cells using an MS2-GFP coat protein. The system utilizes bacteriophage MS2 operator hairpin and coat protein. The coat protein selectively binds to the operator hairpin allowing for specific labeling (Bertrand et al., 1998).

In this system, the sequence of aptamers (MS2 Hairpins) that recognize the MS2 coat protein is added to the untranslated region of the target RNA. The cells are transfected with this construct and the expression construct for the MS2 coat protein fused to GFP. Expression of the tagged RNA can now be visualized via the bound MS2-GFP protein. Applying this technique has enabled several insights into the process of mRNA trafficking.

1.5.2 Spinach Aptamer

Protein based imaging systems are useful for tracking and imaging RNA, but their applications are limited by high background from the unbound protein. To avoid these limitations, fluorophore molecules have been developed and aptamers were designed against these fluorophores. Specification of these small molecules require them to be non-toxic, easily permeable, and provide low non-specific binding to cellular components. Fluorophores have been designed to provide all the above criteria and provide a low fluorescence in the free state and provide fluorescence increases upon binding to their specific aptamer. Malachite green is one such fluorophore. The intramolecular motions are restricted upon aptamer binding. This binding and conformation restriction leads to ~2360 times increase in fluorescence (Babendure et al., 2003). When the Hoechst 1c (Sando et al., 2008) small molecule binds with nanomolar affinity, their fluorescence increases 50-60 fold. Recently, a GFP fluorophore analog, 3,5-difluoro-4- hydroxybenzylidene imidazolinone (DFHBI), was discovered. This small

molecule becomes fluorescent when it binds to an RNA aptamer known as Spinach (Paige et al., 2011).

The spinach aptamer has been utilized to image highly abundant RNA like the 5S rRNA in bacterial and mammalian cells and has been applied as a sensor to image intracellular metabolites (Paige et al., 2012). DFHBI also provided a means to visualize the ASH1 gene is *S. cerevisiae* validating this technology in yeast (Guet et al., 2015). Binding of DFHBI to the RNA promotes stabilization of the transducer stem enabling the Spinach RNA to fold and bind DFHBI. Binding of DFHBI to the spinach RNA then causes fluoresces of the small molecule, limiting the background.

1.6 Research Aim

TDP-43 was recently found as the major protein in ubiquitinated inclusions in ALS (Neumann et al., 2006). When TDP-43 toxicity is tested in *dbr1* deleted yeast, the build-up of lariats proves to rescue tdp-43 toxicity by acting as a decoy. Taking the knowledge of bound RNA to TDP-43 stabilized dimerization, TDP-43 toxicity could be rescued by synthetic RNAs. The main aims of this thesis are:

- To demonstrate different aggregation properties of wild type TDP-43 and mutant TDP-43.
- To demonstrate a difference in wild type TDP-43 and mutant TDP-43 toxicity in *S. cerevisiae*.
- To present evidence from yeast spotting assays and confocal microscopy showing how *in vitro* synthesized RNAs affect TDP-43 toxicity in yeast.

Chapter Two: Materials And Methods

2.1 Yeast Strains, Media, and Plasmids

Yeast were obtained from GE Dharmacon. Yeast parental strain BY4730 (catalog # YSC1061) were used for experiments. Yeast cells were grown in rich yeast peptone dextrose media (YPD) or in synthetic media lacking leucine and containing 2% glucose (SD/-Leu), raffinose (SRaf/-Leu), or galactose (SGal/-Leu). 1 liter of YPD was prepared by adding 20 g yeast extract and 10 g peptone to 900 mL H_2O. The solution is then autoclaved for 30 minutes. 100 mL 20% dextrose is then added to the solution before use.

Yeast containing a deletion of the lariat debranching enzyme *dbr1* were obtained from Dharmacon, Inc. (catalog number YSC6273-201926517). Deletion of *dbr1* was further selected for on plates containing YPD+G418 (200 μg/mL). When plasmids containing auxotrophic markers were transformed into *dbr1Δ* cells, cells were selected for on plates containing

A Yeast Gateway Kit (Kit # 1000000011) was obtained from Addgene. The kit containing 285 yeast Gateway destination vectors based on a widely used pRS series of yeast shuttle vectors and contained two commonly used GPD and GAL1 promoter expression systems.

To generate C-terminally DsRed-tagged or GFP-tagged TDP-43 constructs, a PCR protocol was used to amplify TDP-43 without a stop codon and incorporate the Gateway attB1 and attB2 sites. AttB1 and a primer consisting attB2 plus the 3' end of TDP-43 (omitting the stop codon). Q5® High-Fidelity DNA Polymerase was used to perform the site directed mutagenesis. The resulting PCR products were purified using the Zymo Research DNA Clean & Concentrator.

AttB1	5'GGGGACAAGTTTGTACAAAAAAGCAGGCT3'
attB2+3'TDP43	5'ACCACTTTGTACAAGAAAGCTGGGTTCATTCCCCAGCCAGAAGAC3'

To generate a C-terminally DsRed-tagged or GFP-tagged TDP-43 mutant constructs (Figure 9), a PCR protocol was used to amplify the previously described TDP-43 with the desired mutation. One TDP-43 mutant was generated by deleting amino acids 307-414. This C-terminal domain deleted (ΔCTD) mutant proved does not aggregate but still contains RRM1 and RRM2 for binding of RNA/DNA (Johnson et al.,2007). Johnson also found the mutant to be non-toxic in yeast. AttB1 and a primer consisting attB2 plus the coding sequence for amino acids 408-414. Q5® High-Fidelity DNA Polymerase was used to perform the site directed mutagenesis. The resulting PCR products were purified using the Zymo Research DNA Clean & Concentrator.

attB1	5'GGGGACAAGTTTGTACAAAAAAGCAGGCT3'
attB2+3'TDP43	5'ACCACTTTGTACAAGAAAGCTGGGTATTACTACCTTGATTGTT3'

To generate a negative control containing a C-terminal fluorescent protein, a PCR protocol was used to generate the coding sequence for the first 6 amino acids from yeast GAPDH. One primer containing the sequence for attB1 and the first 15 amino acids of

GAPDH. The other primer contained the sequence of attB2 and the first 17 amino acids of GAPDH. The first 15 nucleic acids of primer 1 are the reverse compliment of last 15 nucleic acids of primer 2. PCR was used to anneal the primers.

attB1+5'GAPDH 5'GGGGCAAGTTTGTACAAAAAAGCAGGCTATGATCAGAATTGCT3'

attB2+3'GAPDH 5'GGGGACCACTTTGTACAAGAAAGCTGGGTTAATAGCAATTCTGATCAT3'

The 76 base-pair PCR product (GAPDH segment) was purified by a phenol-chloroform extraction followed by an ethanol precipitation. An equal volume of 25:24:1(v/v/v) phenol/chloroform/isoamyl alcohol was added to the PCR product. The mixture was mixed using a vortex for 30 seconds before being centrifuged for 30 seconds. The aqueous phase was carefully removed by pipette and transferred to a new tube. 3M Sodium acetate was added to the PCR product (final concentration of 0.3M sodium acetate). 2.5 volumes of ice-cold 100% ethanol was then added to the mixture. The solution was then placed at -80^{o}C for at least 15 minutes. The solution was then centrifuged in a fixed angle microcentrifuge at 21,330 RCF for 5 minutes. The supernatant was then removed before1 mL of 70% ethanol was added to the pellet. The tube was mixed by inversion before being centrifuged at 21,330 RCF for 5 minutes in a fixed angle microcentrifuge. The pellet was dried before being resuspended in molecular biology grade H_2O.

Resulting PCR products were shuttled into pDONR221 using a Gateway BP reaction. The BP reaction resulted in pDONR221 containing TDP-43 flanked with attL1 and attL2. Each BP reaction contained: 150 ng PCR product, 150 ng Pdonr221, TE buffer (to 4 µL), and 1 µL BP Clonase II Mix (ThermoFisher catalog # 11789020).

A Gateway LR reaction was the used to shuttle TDP-43 into the Gateway-compatible yeast expression vectors pAG425GAL-ccdB-DsRed (Figure 8) and pAG425GAL-ccdB-eGFP. The fused DsRed fluorescent protein acts a true monomer. This generation of DsRed accomplishes proper localization and a quicker maturation half-life of 40 minutes—improvements on previous tetrameric DsRed proteins which colocalized and had a maturation half-life of 12 hours (Strongin et al., 2007). Each LR reaction contained: 150 ng PCR product, 150 ng destination vector, TE buffer (to 4 μL), and 1 μL LR Clonase II Mix (ThermoFisher catalog #11791100).

To generate constitutively active RNA decoys (Figure 7A), custom DNA flanked by the Gateway attB1 and attB2 was obtained from Integrated DNA Technologies. The open reading frame consisted of two Dengue Virus xrRNA structures, RNA binding domain (Figure 6), spinach aptamer, MS2 hairpins, 3' ENE, and Civ1.2Rz ribozyme. The designed DNA sequences were shuttled into pDONR221 using a Gateway BP reaction. The BP reaction resulted in pDONR221 containing the custom DNA flanked with attL1 and attL2. A Gateway LR reaction was the used to shuttle custom DNA into the Gateway-compatible yeast expression vectors pAG423GPD-ccdB (Figure 8).

Gateway Vector	**TGGTTGGCCA** CACACTTACT **TTGGGCGTGG** CACACTTACA **GGGTTTCGTA** CACACTAACT **GGTTCTCGAT**
JPS_1481 Vector	**GTGTGAATGAAT** ACACACTTACT **GTGTGAATGAAT** CCACACTTACT **GTGTGAATGAAT** TCACACTTACT **GTGTGAATGAAT**

Figure 6: Sequences for binding domains used for RNA decoys. UG rich sequences shown in bold.

RNA decoys were also tested in plasmids previously used to test xrRNA stability (Figure 7B). Two BglII sites were used to remove the previous insert by a single digestion of the backbone. 3 inserts were designed: one insert contained two consecutive

xrRNAs, 12 TG repeat binding domains (Figure 6), a spinach RNA aptamer, and a Cricket paralysis virus IRES. One insert contained two consecutive xrRNAs, a spinach RNA aptamer, and a Cricket paralysis virus IRES. The last insert contained two consecutive mutated xrRNAs (First three nucleotides in the pseudoknot GTC→CAG), 12 TG repeat binding domains, a spinach RNA aptamer, and a Cricket paralysis virus IRES. All 3 inserts are flanked by BglII digest sites to allow ligation with the backbone.

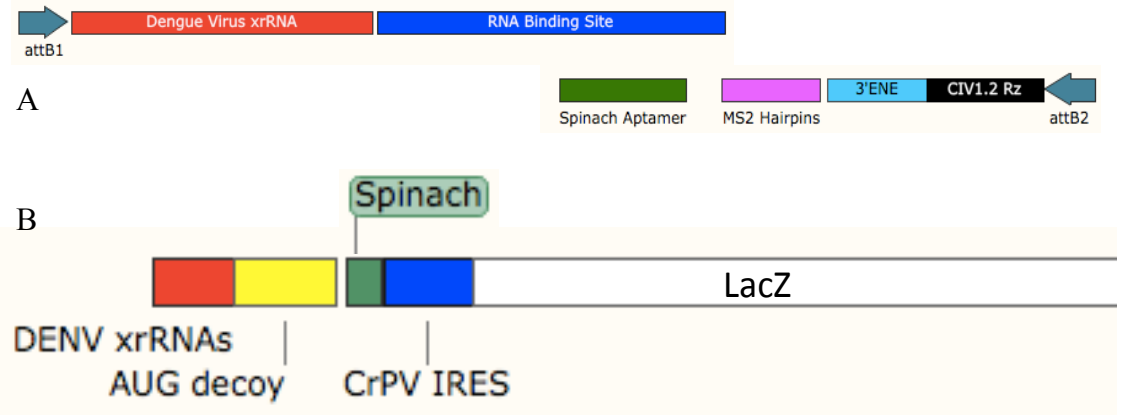

Figure 7: RNA decoy designs used in yeast. **A.** Decoy used in the Gateway system. **B.** Decoy used in the JPS-1481 system. Both designs contain a decay resistant structure, TDP-43 binding site, and aptamer for RNA labeling.

Transformations were performed to obtain yeast containing the generated constructs. Plasmid DNA was transformed using the PEG/lithium acetate method. Yeast were grown to mid-log phase. Yeast were then washed with qH_2O before being resuspended in 100 mM lithium acetate. Finally, yeast cells were resuspended in 50 µL per transformation qH_2O. For each transformation, 50 µL cells were combined with 10µL ssDNA, 1µg DNA, and 500 µL PLATE (40% PEG 3350, 100mM LiOAc, 10 mM TRIS 7.5, and 0.04 mM EDTA). Mixture was heated to 42°C for 40 minutes on a heating

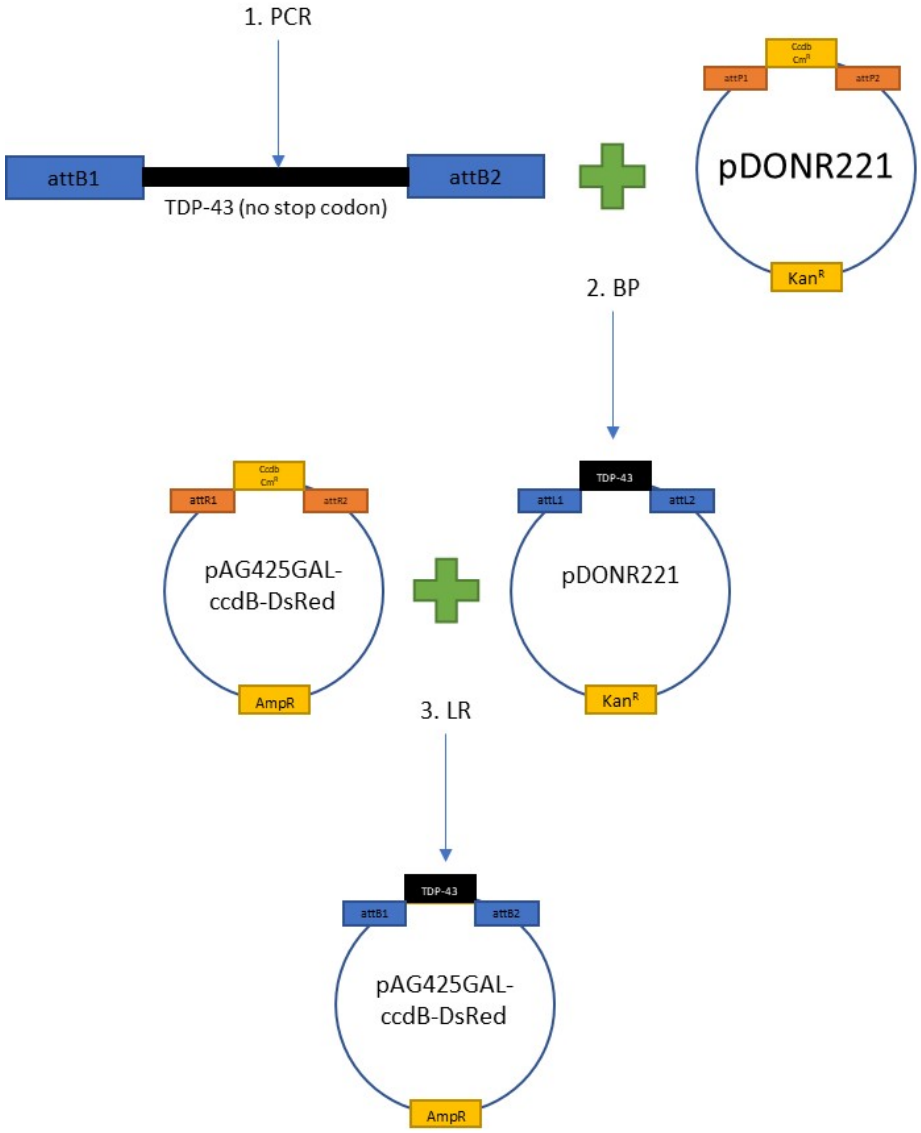

Figure 8: Overview of cloning used to obtain expression vectors. PCR product flanked by attB sites reacts with entry vector with attP sites in a lysogenic (BP) reaction. Resulting product (with attL sites) then reacts with destination vector (attR sites) in a lyctic reaction to produce the expression vector with attB sites.

block. Cells were then plated on a selection media plate depending on the auxotrophic marker. Plates were placed in an incubator for at least 24 hours at 30°C. Culture was then taken and struck on a selection media plate for single colonies.

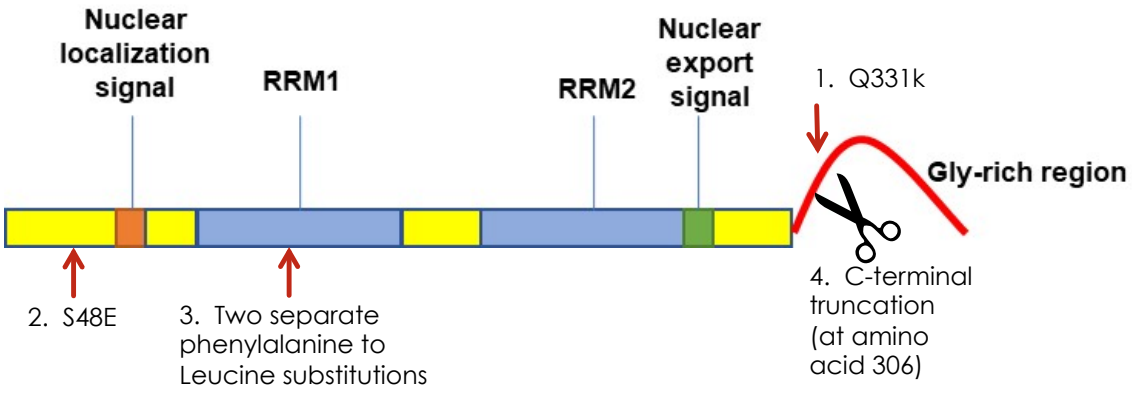

Figure 9: Location of each mutation made and tested. **1.** Lysine to glutamine substitution at residue 331 **2.** Serine to glutamic acid at the 48th residue. **3.** Two separate phenylalanine to leucine substitutions. **4.** C-terminal truncation at amino acid 306.

2.2 Yeast Spotting Assays

To measure cell viability, yeast-spotting assays were performed. Yeast cells were grown overnight at 30°C in synthetic liquid media lacking leucine and containing glucose (Glu/-Leu). 5 mL of fresh SD media were then seeded from the overnight culture (100 µL of overnight culture into 5 mL fresh media) and grown at 30°C until they reached log or mid-log phase. Culture ODs were then normalized, serially diluted in a 96 well plate, and spotted onto synthetic solid media containing glucose or galactose lacking leucine using a V&P Scientific 48 pin Multi-Blot Replicator (cat# VP407AH). The plates were then grown at 30°C for 2–3 days. Pictures were then taken using a ChemiDoc™ MP Imaging System.

2.3 Confocal Microscopy

To visualize TDP-43 aggregates, yeast cells were grown overnight at 30°C in synthetic liquid media lacking leucine and containing raffinose (SRaf/-Leu) until they reached log or mid-log phase. Cells were then spun down at 3426 rcf, resuspended in synthetic media containing glucose or galactose lacking leucine, then incubated at 30°C for 4 or 18 hours. Cells were then fixed using 3.7% formaldehyde for 15 minutes. After fixation, cells were washed twice using phosphate buffered saline. Cells were then permeabilized using 0.1% triton-x for 7 minutes. After permeabilization, cells were washed twice using phosphate buffered saline. Final resuspension of the cells was done in 200 µL PBS. 1 µL of the cell suspension was then combined with 5 µL DAPI mounting media. Cells were cover slipped, sealed with nail polish, and placed in a light protective slide holder. Slides were then imaged on an Olympus FV3000 Confocal Laser Scanning Microscope using a 100x objective. DAPI laser conditions were set at 1% laser power, 700V, 1.0X gain, and 3% offset. Ds-Red laser conditions were set at 0.5% laser power, 510 V, 1.0X gain, and 3% offset.

2.4 Live Cell Imaging

Live cells were imaged to visualize RNA decoys and perform fluorescence recovery after photobleaching (FRAP). Yeast cells were grown overnight at 30°C in synthetic liquid media lacking leucine and containing raffinose (SRaf/-Leu) until they reached log or mid-log phase. 20% glucose or galactose was then added to the cultures to reach a final concentration of 2%. Cultures were then placed back at 30°C for 3.5 hours.

DAPI was then added at a final concentration of 2.5 μg/mL and cultures were placed back at 30°C for 30 minutes. 100 μL cell suspension added to wells coated in concanavalin A. 1 μL of 10 mM DFHBI was thenadded to wells. The plate was then left at 30^{o}C for 20 minutes before removing the top liquid from wells. Wells were then washed with SD media containing 100 μM DFHBI. 100 μL fresh SD media containing 100 μM DFHBI added to wells before imaging. Cells imaged on an Olympus FV3000 Confocal Laser Scanning Microscope using a 100x objective. Ds-Red laser conditions were set at 0.5% laser power, 510 V, 1.0X gain, and 3% offset.

Chapter Three: Results

3.1 Wild Type TDP-43 Toxicity versus TDP-43 mutants

To identify toxicity differences between wild type TDP-43 and mutants of TDP-43, yeast-spotting assays were performed on wild type yeast containing plasmids coding for C-terminally DsRed tagged TDP-43 or a mutant TDP-43 on a galactose promoter. To ensure the DsRed fluorescent protein didn't have a toxic effect on the yeast, the first 6 amino acids of yeast GAPDH were linked to the DsRed fluorescent protein on the C-terminal. Yeast were serially spotted on an auxotrophic selective plate containing glucose (expression off) or galactose (expression on). Spotting on a glucose plate ensured consistent spotting between all test groups and a baseline for no toxicity.

Yeast containing expression plasmids coding for DsRed showed viability equal to yeast on the glucose plate (expression off). TDP-43 showed high levels of toxicity compared to yeast containing plasmids coding for DsRed. Yeast expressing Q331K or S48E showed equal levels of toxicity compared to yeast containing plasmids coding for TDP-43. RRM mutant showed cell viability equal to yeast containing DsRed plasmids. ΔCTD showed lower levels of toxicity compared to TDP-43. Cells still showed lessened cell viability compared to no expression (Figure 10).

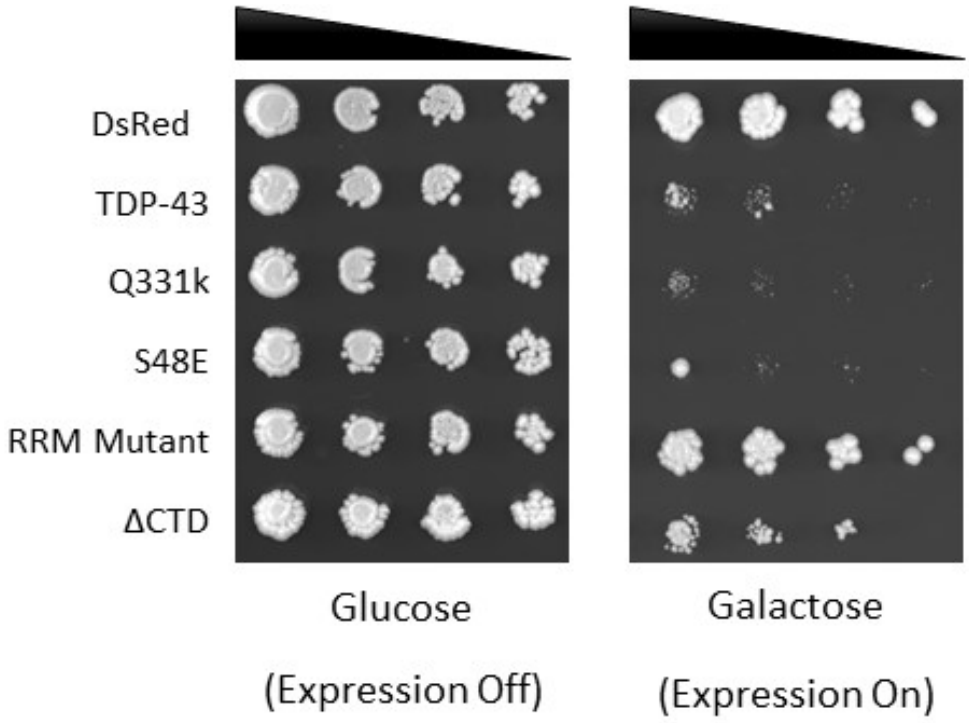

Figure 10: Yeast spotting assay comparing wild type TDP-43 to varous mutants of TDP-43. *Fivefold serial dilution of yeast cells spotted onto glucose (TDP-43 off) or galactose (TDP-43 on).*

3.2 TDP-43 and TDP-43 mutant Toxicity in Wild-Type and *dbr1Δ* Yeast

To identify wild type and mutant TDP-43 toxicity differences in wild type and *dbr1Δ* yeast, yeast-spotting assays were performed with wild type and *dbr1Δ* yeast containing plasmids coding for C-terminally DsRed tagged TDP-43 or a mutant TDP-43 on a galactose promoter. Deletion of the *dbr1* gene previously showed rescue capabilities from TDP-43 toxicity (Johnson et al., 2012). *dbr1Δ* expresses the lariat debranching enzyme which takes part in intron turnover. Without the lariat debranching enzyme, cells can no longer debranch lariats during pre-mRNA splicing. Intronic lariat species accumulate in the cytoplasm of *dbr1*Δ cells and act as decoys to sequester toxic

cytoplasmic TDP-43, possibly preventing it from interfering with other essential cellular RNA targets and RNA-binding proteins.

Yeast containing expression plasmids coding for DsRed showed viability equal to yeast on the glucose plate (expression off) in both wild type and *dbr1Δ* cells. As previously demonstrated, *dbr1Δ* cells showed rescue of TDP-43 toxicity compared to wild type yeast. *dbr1Δ* cells also showed rescue of Q331k toxicity compared to wild type yeast. Cells containing RRM mutant showed cell viability equal to yeast containing DsRed plasmids in both wild type and *dbr1Δ.* ΔCTD showed lower levels of toxicity compared to TDP-43 in both wild type and *dbr1Δ* cells. Complete rescue of ΔCTD toxicity was seen in *dbr1Δ* cells (Figure 11).

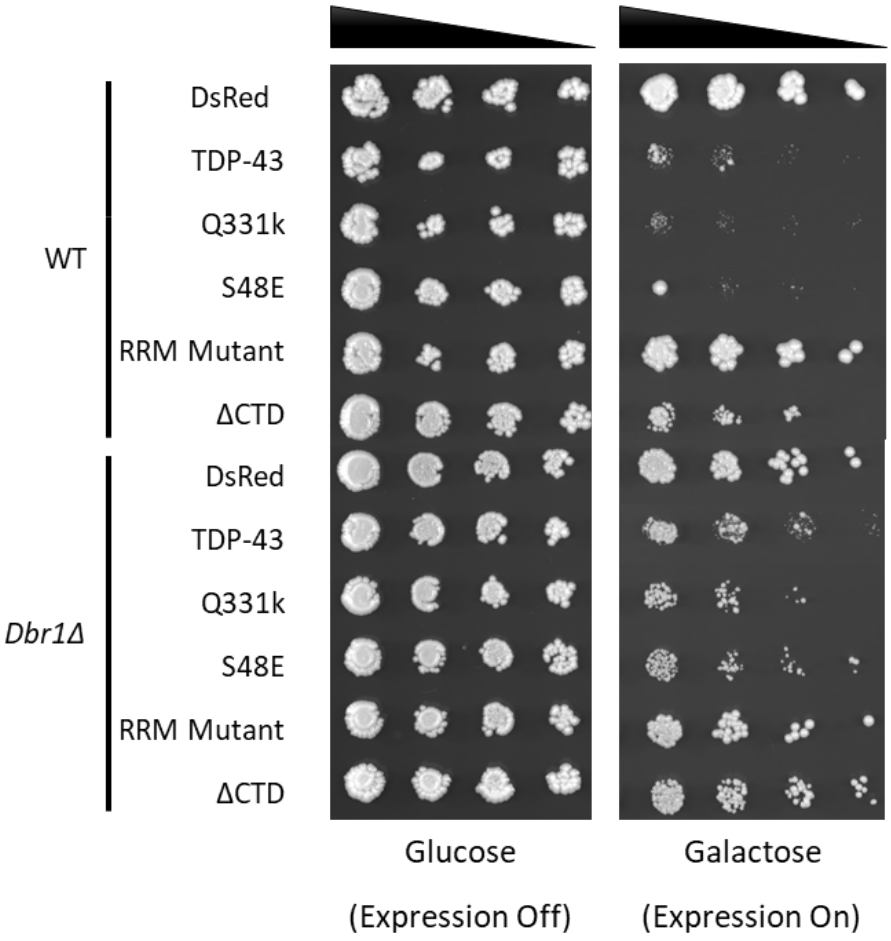

Figure 11: Yeast spotting assay comparing wild type TDP-43 to varous mutants of TDP-43 in wild type and *dbr1Δ yeast*

3.3 Wild Type TDP-43 Aggregation versus TDP-43 mutants

To identify aggregation differences between wild type TDP-43 and mutants of TDP-43, wild type yeast containing plasmids coding for C-terminally DsRed tagged TDP-43 or a mutant TDP-43 on a galactose promoter were observed using a confocal microscope. To ensure the DsRed fluorescent protein didn't aggregate, a construct containing the first 6 amino acids of GAPDH with a C-terminal DsRed tag was also

tested. Yeast were grown to mid-log phase before being resuspended in SD media containing glucose (expression off) or galactose (expression on). Cultures were then grown for 4 or 18 hours before being fixed and permeabilized. 1 μL of cell suspension was added to 5 μL of DAPI mounting media. Cover slides were added and sealed with nail polish. Negative control samples (left in glucose) were used to find appropriate threshold values when preparing images (Figure 12). A sum was taken of all z-stacks in each image. A lower contrast level of 500 relative fluorescent units for the DsRed channel was found appropriate for negative controls. This lower threshold was then used for all images.

After 4-hour induction, wild type TDP-43 and Q331K show cytoplasmic inclusions when highly expressed in the cell. Wild type TDP-43 show fewer puncta per cell compared to Q331K (Figure 13). 18-hour inductions of Q331K result in fewer, but larger, cytoplasmic inclusions. Wild type TDP-43 inclusions after an 18-hour induction are more similar in aggregation tendacies to Q331K after a 4-hour induction (Figure 14).

Cells containing RRM mutant expression plasmids display a very unusual localization. Aggregates form bright, round cytoplasmic structures. Increasing induction time from 4 to 18 hours results in an increase in inclusion size. Cells often contain a single inclusion (Figure 13 and 14).

S48E and ΔCTD showed similar nuclear localization after a 4-hour induction. Cells expressing protein show overlap of DsRed and DAPI staining. Cytoplasmic TDP-43 remains diffuse (Figure 13). 18-hour images of S48E show a single, large aggregate

overlapping, but larger in size, with the nucleus. 18-hour images of ΔCTD still show diffuse cytoplasmic protein with nuclear localization (Figure 14).

3.4 TDP-43 and TDP-43 mutant Aggregation in Wild-Type and *dbr1Δ* Yeast

To identify wild type and mutant TDP-43 aggregation differences in wild type and *dbr1Δ* yeast, wild type and *dbr1Δ* yeast containing plasmids coding for C-terminally DsRed tagged TDP-43 or a mutant TDP-43 on a galactose promoter were observed using a confocal microscope. Deletion of the *dbr1* gene previously showed prevention of multiple, irregular shaped aggregates (Johnson et al., 2012). Aggregates instead formed round singular cytoplasmic inclusions.

After a 4-hour induction, cells containing TDP-43 and Q331K agree with the previous findings in *dbr1Δ* yeast. Singular round cytoplasmic inclusions are oberserved. Cells containing S48E, RRM mut, and ΔCTD show no differences between wild type and *dbr1Δ* yeast after a 4-hour induction (Figure 15 and 16).

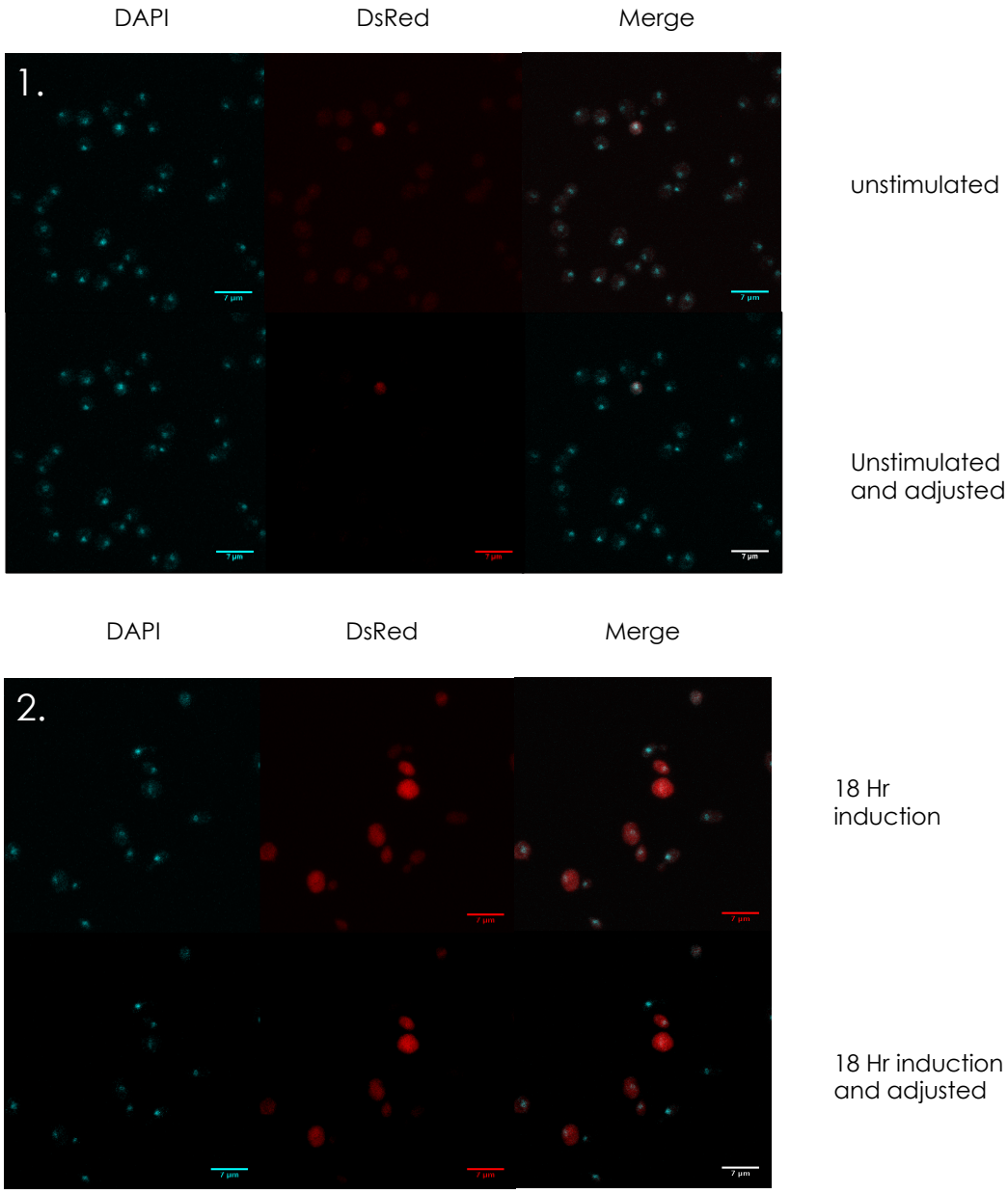

Figure 12: Yeast containing DsRed on a galactose promotor. 1. Unstimulated cultures before and after contrast adjustment. Background is effectively removed after lower contrast was set to 500. 2. Stimulated cultures before and after contrast adjustment. Yeast still show high levels of diffuse DsRed after adjustment.

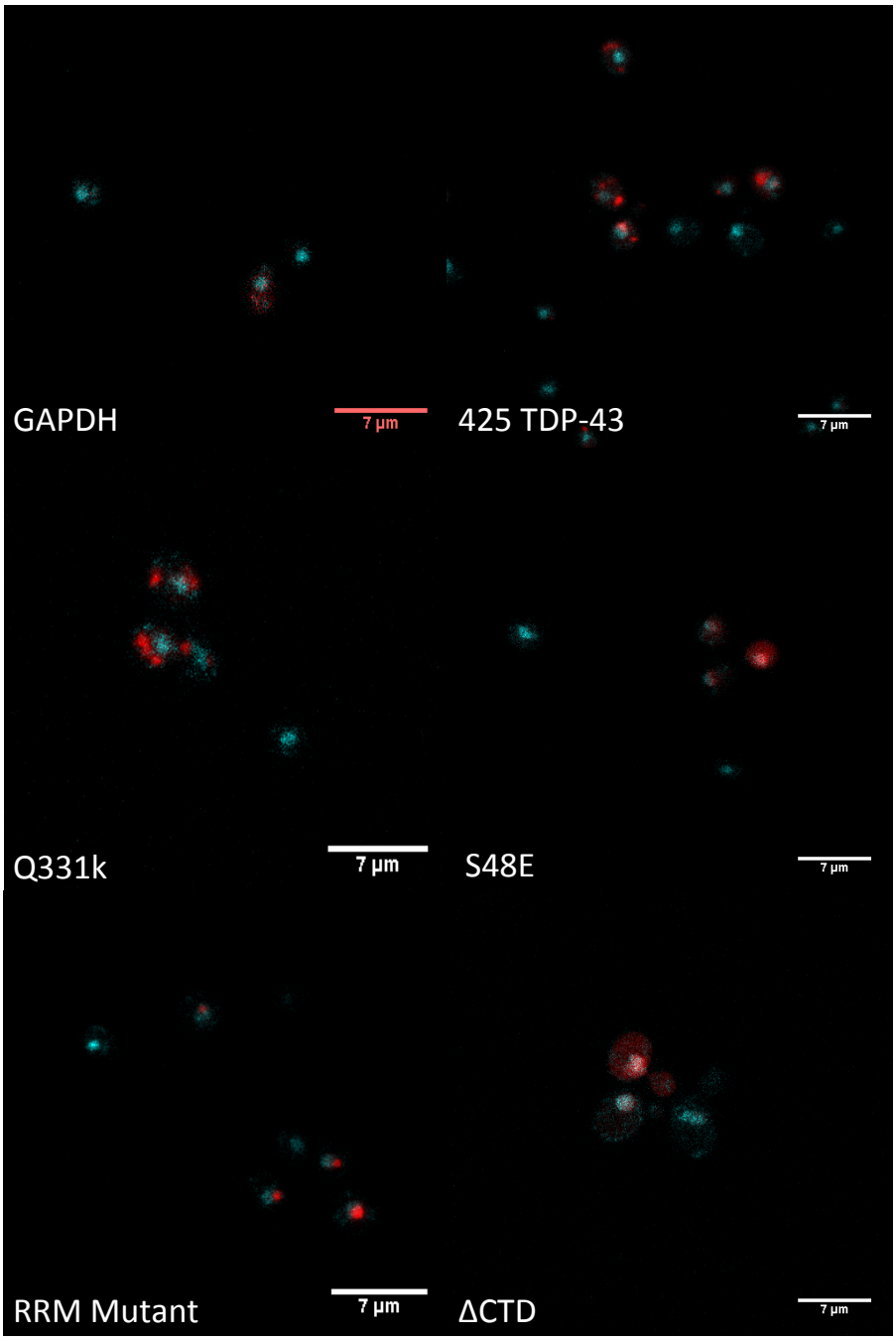

Figure 13: Confocal imaging comparing wild type TDP-43 to varous mutants of TDP-43 in wild type yeast after 4 hours of induction in media containing galactose

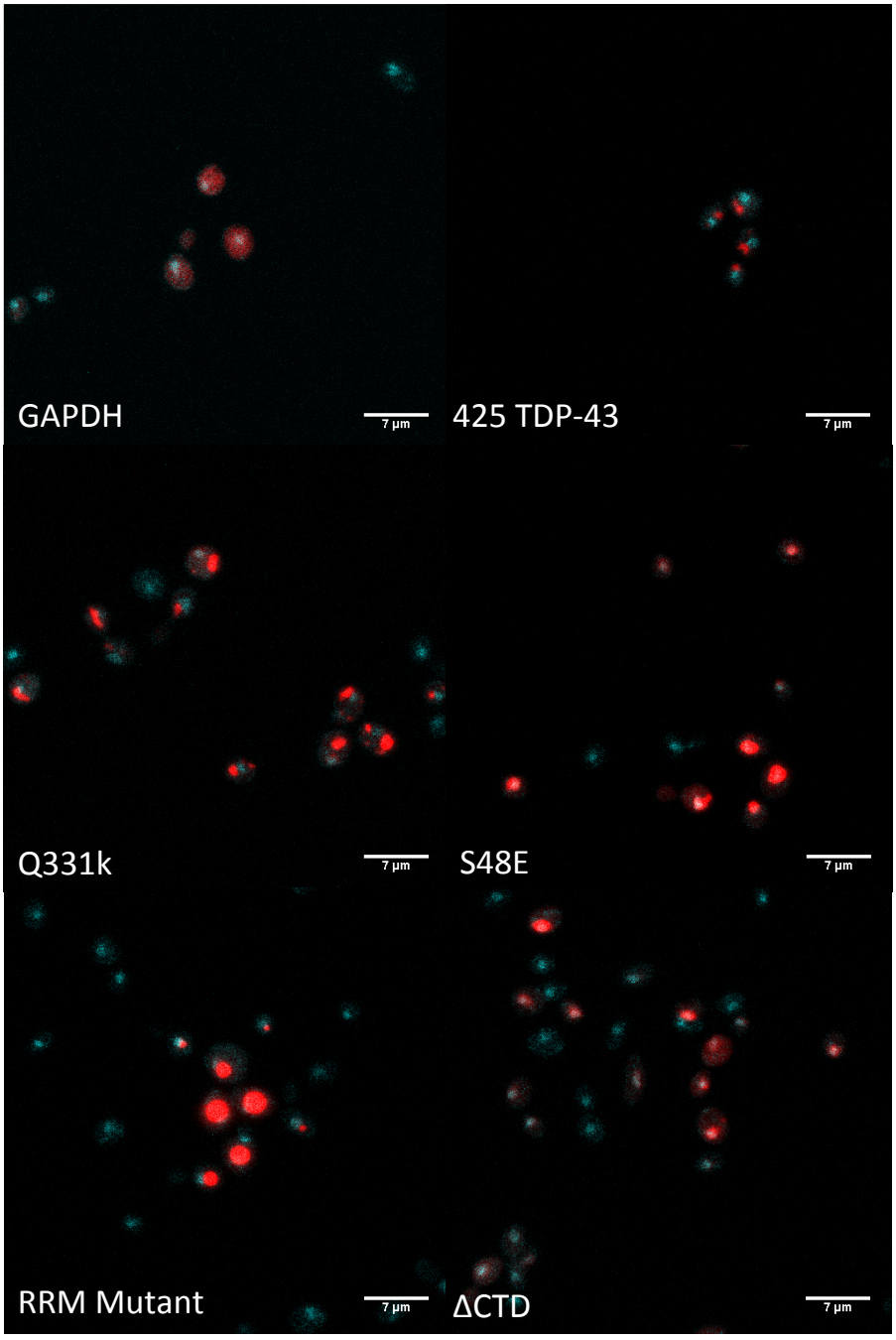

Figure 14: Confocal imaging comparing wild type TDP-43 to varous mutants of TDP-43 in wild type yeast after 18 hours of induction in media containing galactose.

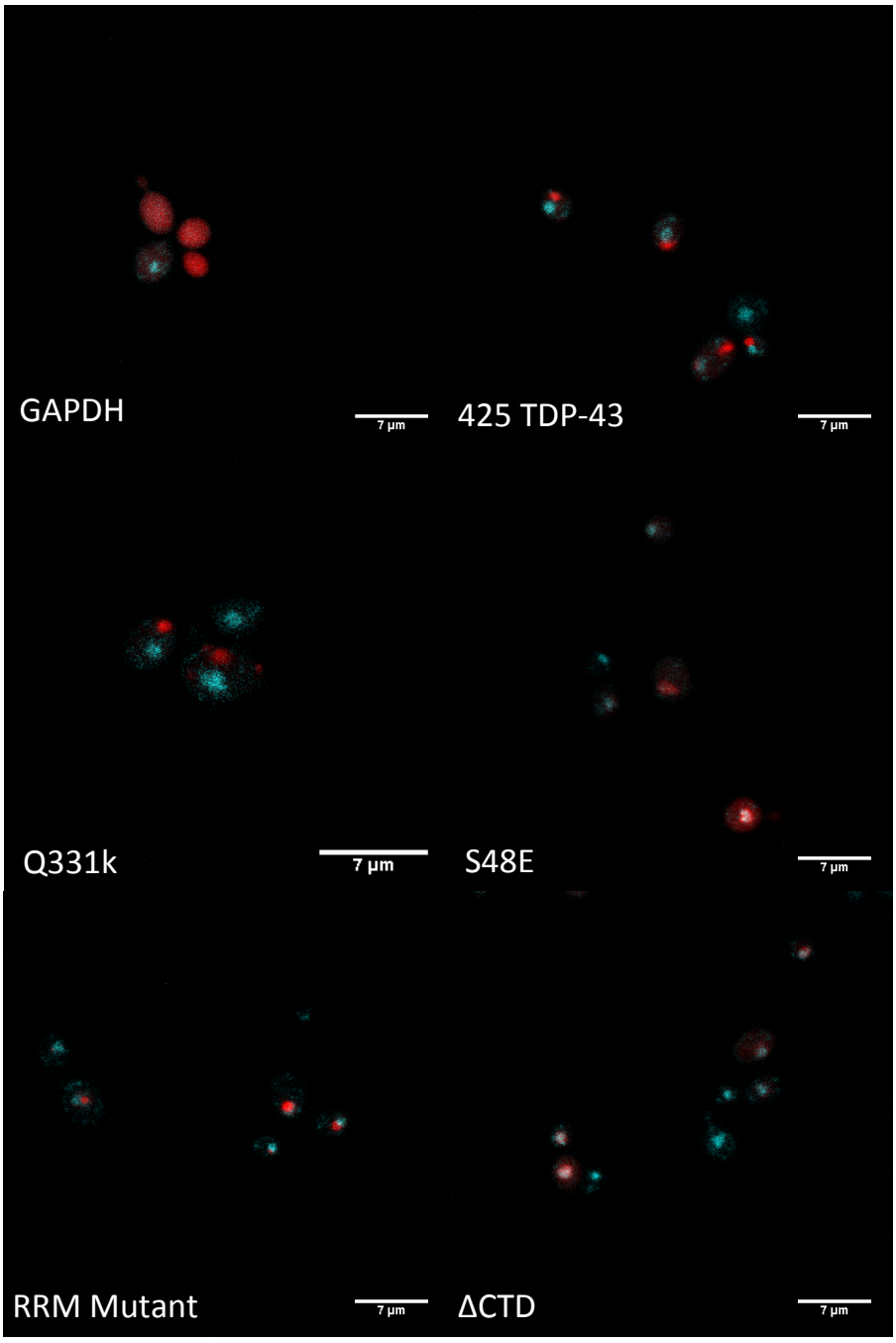

Figure 15: Confocal imaging comparing wild type TDP-43 to varous mutants of TDP-43 in dbr1Δ yeast after 4 hours of induction in media containing galactose.

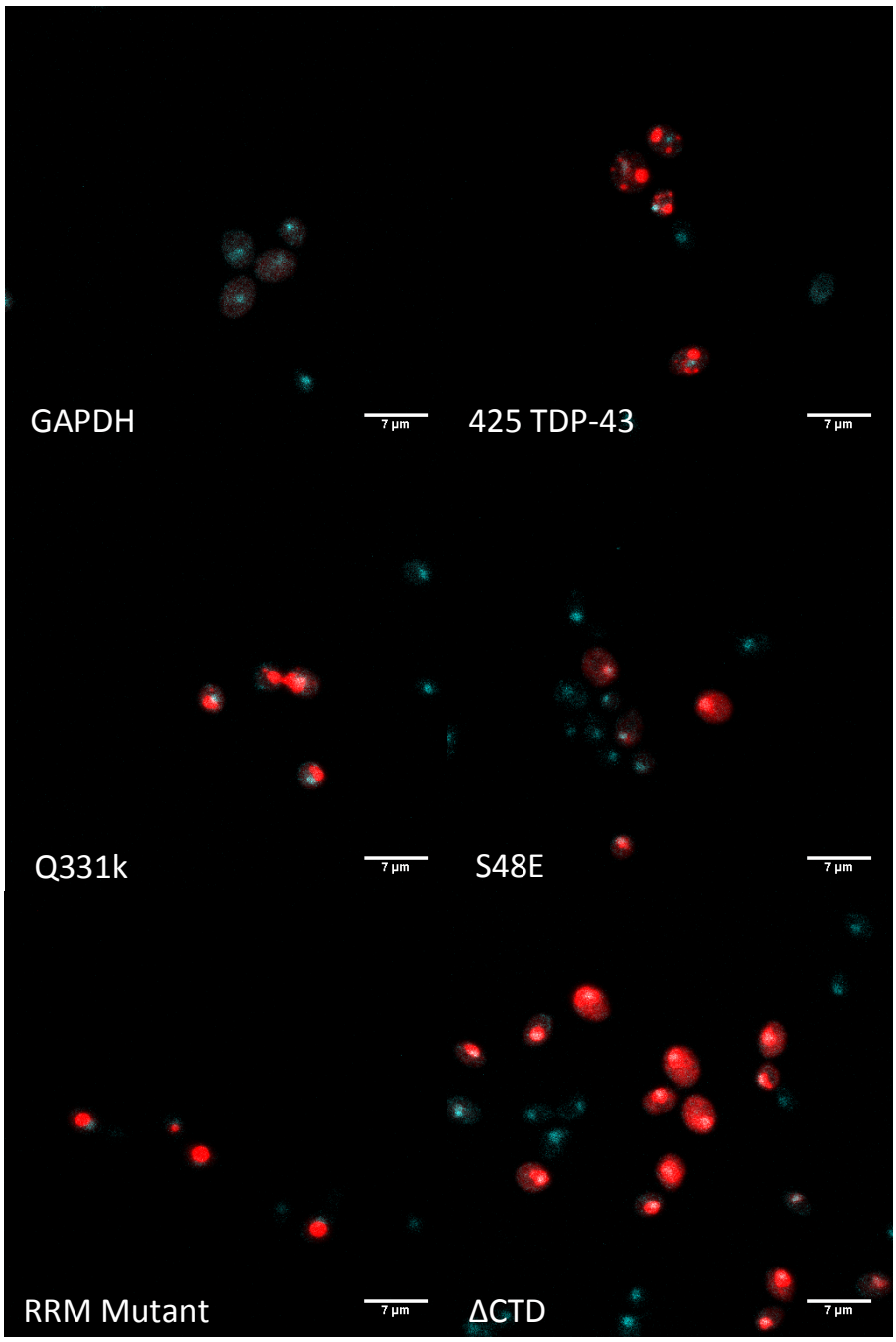

Figure 16: Confocal imaging comparing wild type TDP-43 to varous mutants of TDP-43 in dbr1Δ yeast after 18 hours of induction in media containing galactose.

3.5 Wild Type and RRM Mutant FRAP

RRM mutant and wild type aggregates were photobleached to observe the dynamics of the inclusion. Aggregates only partly recovered by time=50 seconds (46 seconds after photobleaching. Over the 46 seconds, the RRM mutant aggregate recovered to a larger extent compared to the wild type aggregate (Figure 17). Recovery of fluorescents proves diffusion of labeled TDP-43 and a dynamic state of the inclusion.

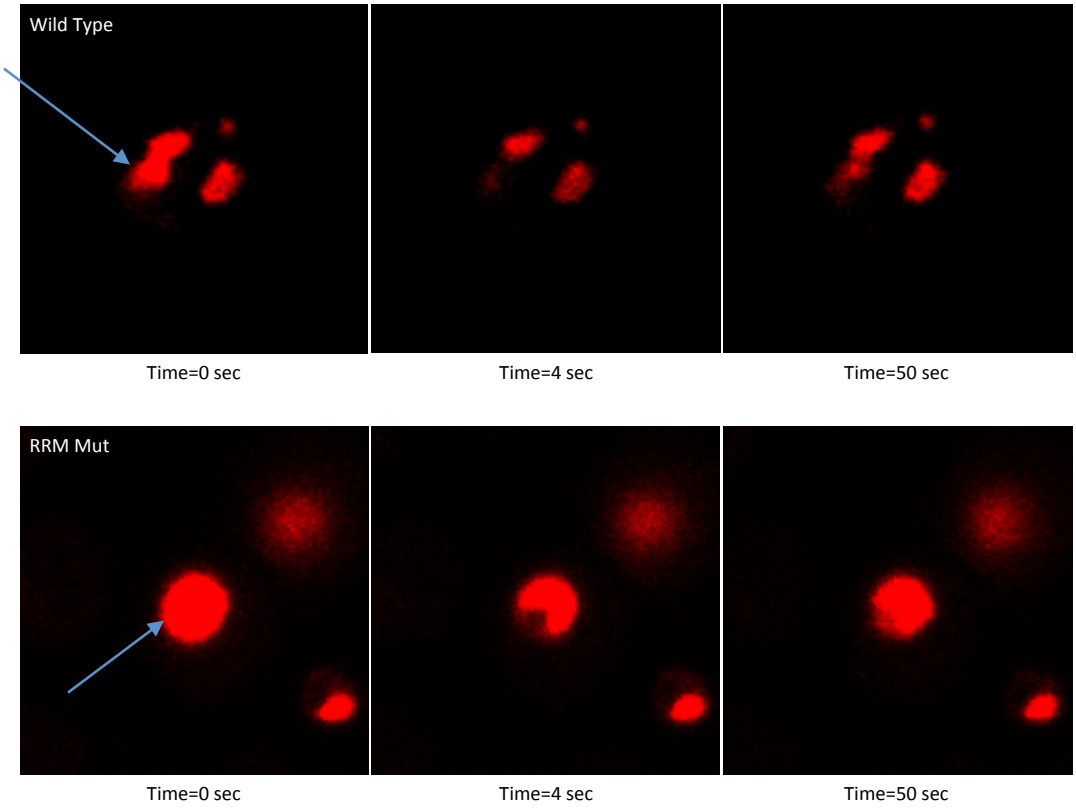

Figure 17: Different timepoints of FRAP experiment. Photobleacing occurred at time=4 seconds.

3.6 Wild Type TDP-43 Aggregation With TDP-43 Decoys

To identify the effects of synthetic RNA on cell viability in yeast containing TDP-43, yeast-spotting assays were performed on wild type yeast containing plasmids coding for C-terminally DsRed tagged TDP-43 on a galactose promoter and constitutively active plasmids coding for the synthetic RNA. Cells were tested 3 different synthetic RNAs. The RNAs differed in number of TDP-43 binding domains (UG rich sequences). RNAs contained 1, 5, or 10 binding domains. To ensure the DsRed fluorescent protein didn't have a toxic effect on the yeast, the first 6 amino acids of yeast GAPDH were linked to the DsRed fluorescent protein on the C-terminal. Yeast were serially spotted on an auxotrophic selective plate containing glucose (expression off) or galactose (expression on). Spotting on a glucose plate ensured consistent spotting between all test groups and a baseline for no toxicity. Spotting on a glucose plate also ensure that adding transcription of synthetic RNAs to the yeast doesn't reduce cell viability.

Yeast containing expression plasmids coding for DsRed and empty destination vector showed viability equal to yeast on the glucose plate (expression off). TDP-43 and empty destination vector showed high levels of toxicity compared to yeast containing plasmids coding for DsRed and empty destination vector. Yeast expressing TDP-43 with X_2DSH_2E and $X_2D_{10}SH_2E$ showed equal levels of viability compared to yeast containing plasmids coding for TDP-43 and empty destination vector (Figure 18).

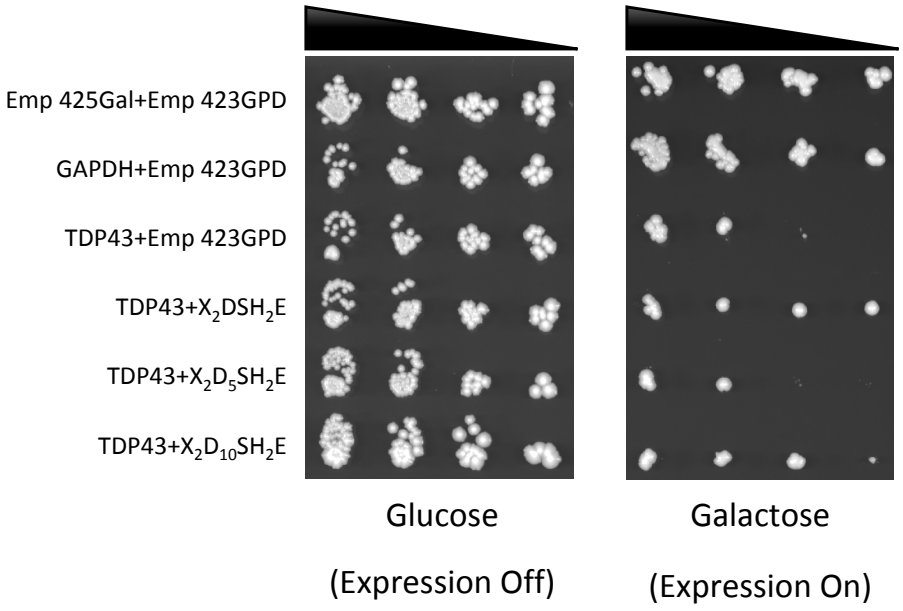

Figure 18: Yeast spotting assay comparing yeast containing TDP-43 with and without syntheticly designed RNA decoys. *Fivefold serial dilution of yeast cells spotted onto glucose (TDP-43 off) or galactose (TDP-43 on).*

Chapter Four: Conclusions

4.1 Thesis Summary

TDP-43 aggregation and cytoplasmic inclusion are hallmarks of non-familial ALS. Distinct pathologies present when mutations of TDP-43 are overexpressed in *S. cerevisiae*. Disruption of the RRM1 by two phenylalanine mutations prevents the ability of TDP-43 to bind RNA by eliminating the ability to form pi-pi stacking in the RRM1 domain (Buratti et al., 2001). Imaging of RRM shows the mutant still aggregates when overexpressed, but yeast spotting assays present evidence the mutation now renders the protein non-toxic. These findings suggest binding and sequestering of RNAs in the cell result in a loss of cell viability.

The C-terminal domain of TDP-43 proves to be important for protein aggregation. Two different mutations in the C-terminal domain were tested. One mutation, Q331K (lysine to glutamine substitution at residue 331), disrupts the alpha helix in the C-terminal. This disruption of the alpha helix significantly disrupts phase separation—stimulating the conversion to aggregates (Conicella et al., 2016). Confocal imaging of Q331K shows more cytoplasmic inclusions per cell compared to wild-type TDP-43 after 4-hour induction. After an 18-hour induction, Q331K inclusions are larger in size than wild type TDP-43. An increased proclivity to aggregate doesn't result in decreased cell viability in yeast spotting assays. Overexpression of both Q331K and wild type TDP-43

show similar levels of toxicity. This result possibly stems from reaching the upper threshold of cytotoxicity. Both wild type TDP-43 and Q331K show almost complete elimination of cell viability. Yeast spotting assays performed with yeast containg wild type TDP-43 and Q331K on low copy plasmids might provide more insight on toxicity differences.

Deletion of the C-terminal domain removes the "prion-like" properties of TDP-43 while leaving the RNA binding ability and selectivity domain alone. The truncation answers an interesting question about the structural influence of TDP-43's toxicity in yeast. Confocal imaging shows a decreased propensity to aggregate. Yeast spotting assays show a decreased toxicity compared to wild-type TDP-43. Aggregation of the protein proves to be an important aspect of the toxicity of TDP-43. Some loss of cell viability was seen in yeast containing the ΔCTD mutant (possibly indicating soluble protein bound to RNA in the cytoplasm still reduces cell viability).

The N-terminal domain of TDP-43 creates the interface in the native dimeric state. Hydrogen bonding and electrostatic forces hold this dimeric state together. Mutation of serine to glutamic acid at the 48th residue disrupts hydrogen bonding in the interface and weakens the assembly of the dimeric state (Wang et al., 2018). Confocal images of S48E after 4 and 18-hour inductions differ greatly. After 4 hours, cells containing S48E show large amount of nuclear protein with diffuse cytoplasmic protein. 18-hour images show a single large aggregate overlapping, but larger in size, with the nucleus. Though differences in aggregation tendencies are observed between wild type

TDP-43 and S48E exist, overexpression results in similar levels of toxicity. Similar to the results of Q331K, yeast-spotting assays performed with yeast containg wild type TDP-43 and S48E on low copy plasmids might provide more insight on toxicity differences.

Preliminary RNA decoy results show present a lack of "rescue" effect by decoys. No difference in cell viability was observed. So far, live cell imaging has failed to capture images of tagged RNAs. JPS_1481 decoys are currently being tested. Since larger UG repeat length result in a larger affinity for TDP-43 binding, the increased binding domain length of 12 nucleotides per binding site in JPS_1481 decoys offers optimism for an increased propensity to co-localize with TDP-43. Based on RRM mutant toxicity data, TDP-43 binding to RNAs drives cellular toxicity (possibly by disrupting critical RNAs in the cytoplasm). Introducing these synthetic RNAs, containing regions TDP-43 preferentially binds, offers hope to rescuing cells from TDP-43 toxicity without genetic modification.

References

(1) Afroz, T.; Hock, E. M.; Ernst, P.; Foglieni, C.; Jambeau, M.; Gilhespy, L. A. B.; Laferriere, F.; Maniecka, Z.; Plückthun, A.; Mittl, P.; et al. Functional and Dynamic Polymerization of the ALS-Linked Protein TDP-43 Antagonizes Its Pathologic Aggregation. *Nat. Commun.* 2017, *8* (1), 45–45.

(2) Armakola, M.; Higgins, M. J.; Figley, M. D.; Barmada, S. J.; Scarborough, E. A.; Diaz, Z.; Fang, X.; Shorter, J.; Krogan, N. J.; Finkbeiner, S.; et al. Inhibition of RNA Lariat Debranching Enzyme Suppresses TDP-43 Toxicity in ALS Disease Models. *Nat. Genet.* 2012, *44* (12), 1302–1309.

(3) Ash, P. E. A.; Zhang, Y. J.; Roberts, C. M.; Saldi, T.; Hutter, H.; Buratti, E.; Petrucelli, L.; Link, C. D. Neurotoxic Effects of TDP-43 Overexpression in C. Elegans. *Hum. Mol. Genet.* 2010, *19* (16), 3206–3218.

(4) Ayala, Y. M.; Misteli, T.; Baralle, F. E. TDP-43 Regulates Retinoblastoma Protein Phosphorylation through the Repression of Cyclin-Dependent Kinase 6 Expression. *Proc. Natl. Acad. Sci.* 2008, *105* (10), 3785–3789.

(5) Ayala, Y. M.; Pantano, S.; D'Ambrogio, A.; Buratti, E.; Brindisi, A.; Marchetti, C.; Romano, M.; Baralle, F. E. Human, Drosophila, and C. Elegans TDP43: Nucleic Acid Binding Properties and Splicing Regulatory Function. *J. Mol. Biol.* 2005, *348* (3), 575–588.

(6) Babendure, J. R.; Adams, S. R.; Tsien, R. Y. Aptamers Switch on Fluorescence of Triphenylmethane Dyes. *J. Am. Chem. Soc.* 2003, *125* (48), 14716–14717.

(7) Banks, G. T.; Kuta, A.; Isaacs, A. M.; Fisher, E. M. C. TDP-43 Is a Culprit in Human Neurodegeneration, and Not Just an Innocent Bystander. *Mammalian Genome*. Springer May 2008, pp 299–305.

(8) Bertrand, E.; Chartrand, P.; Schaefer, M.; Shenoy, S. M.; Singer, R. H.; Long, R. M. Localization of ASH1 MRNA Particles in Living Yeast. *Mol. Cell* 1998, *2* (4), 437–445.

(9) Bhardwaj, A.; Myers, M. P.; Buratti, E.; Baralle, F. E. Characterizing TDP-43 Interaction with Its RNA Targets. *Nucleic Acids Res.* 2013, *41* (9), 5062–5074.

(10) Bhatt, S.; Gething, P. W.; Brady, O. J.; Messina, J. P.; Farlow, A. W.; Moyes, C. L.; Drake, J. M.; Brownstein, J. S.; Hoen, A. G.; Sankoh, O.; et al. The Global Distribution and Burden of Dengue. *Nature* 2013, *496* (7446), 504–507.

(11) Boillée, S.; Vande Velde, C.; Cleveland, D. W. W. ALS: A Disease of Motor Neurons and Their Nonneuronal Neighbors. *Neuron* 2006, *52* (1), 39–59.

(12) Brown, J. A.; Valenstein, M. L.; Yario, T. A.; Tycowski, K. T.; Steitz, J. A. Formation of Triple-Helical Structures by the 3'-End Sequences of MALAT1 and MEN Noncoding RNAs. *Proc. Natl. Acad. Sci.* 2012, *109* (47), 19202–19207.

(13) Bruijn, L. I.; Houseweart, M. K.; Kato, S.; Anderson, K. L.; Anderson, S. D.; Ohama, E.; Reaume, A. G.; Scott, R. W.; Cleveland, D. W. Aggregation and Motor Neuron Toxicity of an ALS-Linked SOD1 Mutant Independent from Wild-Type SOD1. *Science (80-.).* 1998, *281* (5384), 1851–1854.

(14) Buratti, E. Multiple Roles of TDP-43 in Gene Expression, Splicing Regulation, and Human Disease. *Front. Biosci.* 2008, *13* (13), 867.

(15) Buratti, E.; Baralle, F. E. Characterization and Functional Implications of the RNA Binding Properties of Nuclear Factor TDP-43, a Novel Splicing Regulator of CFTR Exon 9. *J. Biol. Chem.* 2001, *276* (39), 36337–36343.

(16) Butler, G. S.; Overall, C. M. Proteomic Identification of Multitasking Proteins in Unexpected Locations Complicates Drug Targeting. *Nat. Rev. Drug Discov.* 2009, *8* (12), 935–948.

(17) Chacinska, A.; Koehler, C. M.; Milenkovic, D.; Lithgow, T.; Pfanner, N. Importing Mitochondrial Proteins: Machineries and Mechanisms. *Cell* 2009, *138* (4), 628–644.

(18) Chambers, T. J.; Hahn, C. S.; Galler, R.; Rice, C. M. AND REPLICATION ORGJ \ NIZATION , EXPRESSION , L. *Annu. Rev. Virol.* 1990, *44*, 649–688.

(19) Chapman, E. G.; Costantino, D. A.; Rabe, J. L.; Moon, S. L.; Wilusz, J.; Nix, J. C.; Kieft, J. S. The Structural Basis of Pathogenic Subgenomic Flavivirus RNA (SfRNA) Production. *Science (80-.).* 2014, *344* (6181), 307–310.

(20) Christianson, T. W.; Sikorski, R. S.; Dante, M.; Shero, J. H.; Hieter, P. Multifunctional Yeast High-Copy-Number Shuttle Vectors. *Gene* 1992, *110* (1), 119–122.

(21) Dansen, T. B.; Burgering, B. M. T. Unravelling the Tumor-Suppressive Functions of FOXO Proteins. *Trends Cell Biol.* 2008, *18* (9), 421–429.

(22) Davidenko, T. I.; Kuznetsova, E. V. Microbiological Hydrolysis of 3-Acetoxy-1,4-Benzodiazepin-2-Ones. *Pharm. Chem. J.* 1980, *13* (4), 412–414.

(23) Diaper, D. C.; Adachi, Y.; Lazarou, L.; Greenstein, M.; Simoes, F. A.; Di Domenico, A.; Solomon, D. A.; Lowe, S.; Alsubaie, R.; Cheng, D.; et al. Drosophila TDP-43 Dysfunction in Glia and Muscle Cells Cause Cytological and Behavioural Phenotypes That Characterize ALS and FTLD. *Hum. Mol. Genet.* 2013, *22* (19), 3883–3893.

(24) Funk, A.; Truong, K.; Nagasaki, T.; Torres, S.; Floden, N.; Balmori Melian, E.; Edmonds, J.; Dong, H.; Shi, P.-Y.; Khromykh, A. A. RNA Structures Required for Production of Subgenomic Flavivirus RNA. *J. Virol.* 2010, *84* (21), 11407–11417.

(25) Giaever, G.; Chu, A. M.; Ni, L.; Connelly, C.; Riles, L.; Véronneau, S.; Dow, S.; Lucau-Danila, A.; Anderson, K.; André, B.; et al. Functional Profiling of the Saccharomyces Cerevisiae Genome. *Nature* 2002, *418* (6896), 387–391.

(26) Gitcho, M. A.; Baloh, R. H.; Chakraverty, S.; Mayo, K.; Norton, J. B.; Levitch, D.; Hatanpaa, K. J.; White, C. L.; Bigio, E. H.; Caselli, R.; et al. TDP-43 A315T Mutation in Familial Motor Neuron Disease. *Ann. Neurol.* 2008, *63* (4), 535–538.

(27) Gitler, A. D.; Shorter, J. RNA-Binding Proteins with Prion-like Domains in ALS and FTLD-U. *Prion*. Taylor & Francis July 4, 2011, pp 179–187.

(28) Guet, D.; Burns, L. T.; Maji, S.; Boulanger, J.; Hersen, P.; Wente, S. R.; Salamero, J.; Dargemont, C. Combining Spinach-Tagged RNA and Gene Localization to Image Gene Expression in Live Yeast. *Nat. Commun.* 2015, *6* (1), 8882.

(29) Ho, H. O. *A HO HO N N O O O DMHBI HBI (in GFP) Downloaded From*.

(30) Huang, Y. C.; Lin, K. F.; He, R. Y.; Tu, P. H.; Koubek, J.; Hsu, Y. C.; Huang, J. J. T. Inhibition of TDP-43 Aggregation by Nucleic Acid Binding. *PLoS One* 2013, *8* (5), e64002.

(31) Hung, M.-C.; Link, W. Protein Localization in Disease and Therapy. *J. Cell Sci.* 2011, *124* (20), 3381–3392.

(32) Iguchi, Y.; Katsuno, M.; Niwa, J. I.; Takagi, S.; Ishigaki, S.; Ikenaka, K.; Kawai, K.; Watanabe, H.; Yamanaka, K.; Takahashi, R.; et al. Loss of TDP-43 Causes

Age-Dependent Progressive Motor Neuron Degeneration. *Brain* 2013, *136* (5), 1371–1382.

(33) Johnson, B. S.; McCaffery, J. M.; Lindquist, S.; Gitler, A. D. A Yeast TDP-43 Proteinopathy Model: Exploring the Molecular Determinants of TDP-43 Aggregation and Cellular Toxicity. *Proc. Natl. Acad. Sci.* 2008, *105* (17), 6439–6444.

(34) Johnson, B. S.; Snead, D.; Lee, J. J.; McCaffery, J. M.; Shorter, J.; Gitler, A. D. TDP-43 Is Intrinsically Aggregation-Prone, and Amyotrophic Lateral Sclerosis-Linked Mutations Accelerate Aggregation and Increase Toxicity. *J. Biol. Chem.* 2009, *284* (30), 20329–20339.

(35) Jones, C. I.; Zabolotskaya, M. V.; Newbury, S. F. The 5′ → 3′ Exoribonuclease XRN1/Pacman and Its Functions in Cellular Processes and Development. *Wiley Interdisciplinary Reviews: RNA*. John Wiley & Sons, Inc. July 1, 2012, pp 455–468.

(36) Kabashi, E.; Lin, L.; Tradewell, M. L.; Dion, P. A.; Bercier, V.; Bourgouin, P.; Rochefort, D.; Bel Hadj, S.; Durham, H. D.; Velde, C. Vande; et al. Gain and Loss of Function of ALS-Related Mutations of TARDBP (TDP-43) Cause Motor Deficits in Vivo. *Hum. Mol. Genet.* 2009, *19* (4), 671–683.

(37) Kabashi, E.; Valdmanis, P. N.; Dion, P.; Spiegelman, D.; McConkey, B. J.; Velde, C. Vande; Bouchard, J. P.; Lacomblez, L.; Pochigaeva, K.; Salachas, F.; et al. TARDBP Mutations in Individuals with Sporadic and Familial Amyotrophic Lateral Sclerosis. *Nat. Genet.* 2008, *40* (5), 572–574.

(38) King, O. D.; Gitler, A. D.; Shorter, J. The Tip of the Iceberg: RNA-Binding Proteins with Prion-like Domains in Neurodegenerative Disease. *Brain Res.* 2012, *1462*, 61–80.

(39) Kraemer, B. C.; Schuck, T.; Wheeler, J. M.; Robinson, L. C.; Trojanowski, J. Q.; Lee, V. M. Y.; Schellenberg, G. D. Loss of Murine TDP-43 Disrupts Motor Function and Plays an Essential Role in Embryogenesis. *Acta Neuropathol.* 2010, *119* (4), 409–419.

(40) Kuo, P. H.; Doudeva, L. G.; Wang, Y. T.; Shen, C. K. J.; Yuan, H. S. Structural Insights into TDP-43 in Nucleic-Acid Binding and Domain Interactions. *Nucleic Acids Res.* 2009, *37* (6), 1799–1808.

(41) Lagier-Tourenne, C.; Polymenidou, M.; Cleveland, D. W. TDP-43 and FUS/TLS: Emerging Roles in RNA Processing and Neurodegeneration. *Hum. Mol. Genet.* 2010, *19* (R1), R46–R64.

(42) Lescoute, A.; Westhof, E. Topology of Three-Way Junctions in Folded RNAs. *Rna* 2006, *12* (1), 83–93.

(43) Li, H. R.; Chiang, W. C.; Chou, P. C.; Wang, W. J.; Huang, J. rong. TAR DNA-Binding Protein 43 (TDP-43) Liquid-Liquid Phase Separation Is Mediated by Just a Few Aromatic Residues. *J. Biol. Chem.* 2018, *293* (16), 6090–6098.

(44) Li, Y.; Ray, P.; Rao, E. J.; Shi, C.; Guo, W.; Chen, X.; Woodruff, E. A.; Fushimi, K.; Wu, J. Y. A Drosophila Model for TDP-43 Proteinopathy. *Proc. Natl. Acad. Sci.* 2010, *107* (7), 3169–3174.

(45) Mackenzie, I. R. A.; Bigio, E. H.; Ince, P. G.; Geser, F.; Neumann, M.; Cairns, N. J.; Kwong, L. K.; Forman, M. S.; Ravits, J.; Stewart, H.; et al. Pathological TDP-43 Distinguishes Sporadic Amyotrophic Lateral Sclerosis from Amyotrophic Lateral Sclerosis with SOD1 Mutations. *Ann. Neurol.* 2007, *61* (5), 427–434.

(46) Mackenzie, J. S.; Gubler, D. J.; Petersen, L. R. Emerging Flaviviruses: The Spread and Resurgence of Japanese Encephalitis, West Nile and Dengue Viruses. *Nature Medicine*. Nature Publishing Group December 30, 2004, pp S98–S109.

(47) Maekawa, S.; Leigh, P. N.; King, A.; Jones, E.; Steele, J. C.; Bodi, I.; Shaw, C. E.; Hortobagyi, T.; Al-Sarraj, S. TDP-43 Is Consistently Co-Localized with Ubiquitinated Inclusions in Sporadic and Guam Amyotrophic Lateral Sclerosis but Not in Familial Amyotrophic Lateral Sclerosis with and without SOD1 Mutations. *Neuropathology* 2009, *29* (6), 672–683.

(48) Mayer, G. The Chemical Biology of Aptamers. *Angew. Chemie - Int. Ed.* 2009, *48* (15), 2672–2689.

(49) McKeague, M.; Derosa, M. C. Challenges and Opportunities for Small Molecule Aptamer Development. *J. Nucleic Acids* 2012, *2012*.

(50) McLane, L. M.; Corbett, A. H. Nuclear Localization Signals and Human Disease. *IUBMB Life* 2009, *61* (7), 697–706.

(51) Molliex, A.; Temirov, J.; Lee, J.; Coughlin, M.; Anderson, P.; Kim, H. J.; Mittag, T.; Taylor, J. P. Phase Separation by Low Complexity Domains Promotes Stress Granule Assembly and Drives Pathological Fibrillization. 2015, *163* (1), 123–133.

(52) Normile, D. Tropical Medicine. Surprising New Dengue Virus Throws a Spanner in Disease Control Efforts. *Science (New York, N.Y.)*. American Association for the Advancement of Science October 25, 2013, p 415.

(53) Paige, J. S.; Nguyen-Duc, T.; Song, W.; Jaffrey, S. R. Fluorescence Imaging of Cellular Metabolites with RNA. *Science*. 2012.

(54) Pesiridis, G. S.; Lee, V. M. Y.; Trojanowski, J. Q. Mutations in TDP-43 Link Glycine-Rich Domain Functions to Amyotrophic Lateral Sclerosis. *Hum. Mol. Genet.* 2009, *18* (R2), R156–R162.

(55) Pesiridis, G. S.; Tripathy, K.; Tanik, S.; Trojanowski, J. Q.; Lee, V. M. Y. A "Two-Hit" Hypothesis for Inclusion Formation by Carboxyl-Terminal Fragments of TDP-43 Protein Linked to RNA Depletion and Impaired Microtubule-Dependent Transport. *J. Biol. Chem.* 2011, *286* (21), 18845–18855.

(56) Pijlman, G. P.; Funk, A.; Kondratieva, N.; Leung, J.; Torres, S.; van der Aa, L.; Liu, W. J.; Palmenberg, A. C.; Shi, P. Y.; Hall, R. A.; et al. A Highly Structured, Nuclease-Resistant, Noncoding RNA Produced by Flaviviruses Is Required for Pathogenicity. *Cell Host Microbe* 2008, *4* (6), 579–591.

(57) Plum, G. E.; Park, Y. W.; Singleton, S. F.; Dervan, P. B.; Breslauer, K. J. Thermodynamic Characterization of the Stability and the Melting Behavior of a DNA Triplex: A Spectroscopic and Calorimetric Study. *Proc. Natl. Acad. Sci.* 1990, *87* (23), 9436–9440.

(58) Roemer, J. E. Equaltiy of Opportunity. *New Palgrave Dict.* 2005, *64* (1), 1–17.

(59) Rosen, D. R.; Siddique, T.; Patterson, D.; Figlewicz, D. A.; Sapp, P.; Hentati, A.; Donaldson, D.; Goto, J.; O'Regan, J. P.; Deng, H.-X.; et al. Mutations in Cu/Zn Superoxide Dismutase Gene Are Associated with Familial Amyotrophic Lateral Sclerosis. *Nature* 1993, *362* (6415), 59–62.

(60) Ross, C. A.; Poirier, M. A. Protein Aggregation and Neurodegenerative Disease. *Nat. Med.* 2004, *10* (7), S10.

(61) Rutherford, N. J.; Zhang, Y.-J.; Baker, M.; Gass, J. M.; Finch, N. A.; Xu, Y.-F.; Stewart, H.; Kelley, B. J.; Kuntz, K.; Crook, R. J. P.; et al. Novel Mutations in TARDBP (TDP-43) in Patients with Familial Amyotrophic Lateral Sclerosis. *PLoS Genet.* 2008, *4* (9), e1000193.

(62) Sando, S.; Narita, A.; Hayami, M.; Aoyama, Y. Transcription Monitoring Using Fused RNA with a Dye-Binding Light-up Aptamer as a Tag: A Blue Fluorescent RNA. *Chem. Commun.* 2008.

(63) Schmidt, H. B.; Rohatgi, R. In Vivo Formation of Vacuolated Multi-Phase Report In Vivo Formation of Vacuolated Multi-Phase Compartments Lacking Membranes. *CellReports* 2016, *16* (5), 1228–1236.

(64) Sephton, C. F.; Good, S. K.; Atkin, S.; Dewey, C. M.; Mayer, P.; Herz, J.; Yu, G. TDP-43 Is a Developmentally Regulated Protein Essential for Early Embryonic Development. *J. Biol. Chem.* 2010, *285* (9), 6826–6834.

(65) Shiina, Y.; Arima, K.; Tabunoki, H. TDP-43 Dimerizes in Human Cells in Culture. 2010, 641–652.

(66) Siddique, T.; Ajroud-Driss, S. Familial Amyotrophic Lateral Sclerosis, a Historical Perspective. *Acta Myol.* 2011, *30* (2), 117–120.

(67) Sikorski, R. S.; Hieter, P. A System of Shuttle Vectors and Yeast Host Strains Designed for Efficient Manipulation of DNA In. 1989, No. 1 979.

(68) Smith, R. A.; Miller, T. M.; Yamanaka, K.; Monia, B. P.; Condon, T. P.; Hung, G.; Lobsiger, C. S.; Ward, C. M.; McAlonis-Downes, M.; Wei, H.; et al. Antisense Oligonucleotide Therapy for Neurodegenerative Disease. *J. Clin. Invest.* 2006, *116* (8), 2290–2296.

(69) Sreedharan, J.; Blair, I. P.; Tripathi, V. B.; Hu, X.; Vance, C.; Rogelj, B.; Ackerley, S.; Durnall, J. C.; Williams, K. L.; Buratti, E.; et al. TDP-43 Mutations in Familial and Sporadic Amyotrophic Lateral Sclerosis. *Science (80-.).* 2008, *319* (5870), 1668–1672.

(70) Strongin, D. E.; Bevis, B.; Khuong, N.; Downing, M. E.; Strack, R. L.; Sundaram, K.; Glick, B. S.; Keenan, R. J. Structural Rearrangements near the Chromophore Influence the Maturation Speed and Brightness of DsRed Variants. *Protein Eng. Des. Sel.* 2007, *20* (11), 525–534.

(71) Sun, Y.; Arslan, P. E.; Won, A.; Yip, C. M.; Chakrabartty, A. Binding of TDP-43 to the 3′UTR of Its Cognate MRNA Enhances Its Solubility. *Biochemistry* 2014, *53* (37), 5885–5894.

(72) Sun, Y.; Chakrabartty, A. Phase to Phase with TDP-43. *Biochemistry* 2017, *56* (6), 809–823.

(73) Taylor, J. P.; Cleveland, D. W. Decoding ALS: From Genes to Mechanism. 2017, *539* (7628), 197–206.

(74) Van Blitterswijk, M.; DeJesus-Hernandez, M.; Rademakers, R. How Do C9ORF72 Repeat Expansions Cause ALS and FTD: Can We Learn from Other Non-Coding Repeat Expansion Disorders? Marka. *Curr Opin Neurol* 2012, *25* (6), 689–700.

(75) Van Deerlin, V. M.; Leverenz, J. B.; Bekris, L. M.; Bird, T. D.; Yuan, W.; Elman, L. B.; Clay, D.; Wood, E. M. C.; Chen-Plotkin, A. S.; Martinez-Lage, M.; et al. TARDBP Mutations in Amyotrophic Lateral Sclerosis with TDP-43 Neuropathology: A Genetic and Histopathological Analysis. *Lancet Neurol.* 2008, *7* (5), 409–416.

(76) van Es, M. A.; Hardiman, O.; Chio, A.; Al-Chalabi, A.; Pasterkamp, R. J.; Veldink, J. H.; van den Berg, L. H. Amyotrophic Lateral Sclerosis. *Lancet* 2017, *390* (10107), 2084–2098.

(77) Wang, A.; Conicella, A. E.; Schmidt, H. B.; Martin, E. W.; Rhoads, S. N.; Reeb, A. N.; Nourse, A.; Ramirez Montero, D.; Ryan, V. H.; Rohatgi, R.; et al. A Single N□terminal Phosphomimic Disrupts TDP□43 Polymerization, Phase Separation, and RNA Splicing. *EMBO J.* 2018.

(78) Wang, T.; Ray, J. Aptamer-Based Molecular Imaging. 2012, *3* (10), 739–754.

(79) Wils, H.; Kleinberger, G.; Janssens, J.; Pereson, S.; Joris, G.; Cuijt, I.; Smits, V.; Ceuterick-de Groote, C.; Van Broeckhoven, C.; Kumar-Singh, S. TDP-43 Transgenic Mice Develop Spastic Paralysis and Neuronal Inclusions Characteristic of ALS and Frontotemporal Lobar Degeneration. *Proc. Natl. Acad. Sci.* 2010, *107* (8), 3858–3863.

(80) Winton, M. J.; Igaz, L. M.; Wong, M. M.; Kwong, L. K.; Trojanowski, J. Q.; Lee, V. M. Y. Disturbance of Nuclear and Cytoplasmic TAR DNA-Binding Protein (TDP-43) Induces Disease-like Redistribution, Sequestration, and Aggregate Formation. *J. Biol. Chem.* 2008, *283* (19), 13302–13309.

(81) Wu, L. S.; Cheng, W. C.; Shen, C. K. J. Targeted Depletion of TDP-43 Expression in the Spinal Cord Motor Neurons Leads to the Development of Amyotrophic Lateral Sclerosis-like Phenotypes in Mice. *J. Biol. Chem.* 2012, *287* (33), 27335–27344.

(82) Wu, L.-S.; Cheng, W.-C.; Hou, S.-C.; Yan, Y.-T.; Jiang, S.-T.; Shen, C.-K. J. TDP-43, a Neuro-Pathosignature Factor, Is Essential for Early Mouse Embryogenesis. *Genesis* 2009, *48* (1), n/a-n/a.

(83) Yang, C.; Wang, H.; Qiao, T.; Yang, B.; Aliaga, L.; Qiu, L.; Tan, W.; Salameh, J.; McKenna-Yasek, D. M.; Smith, T.; et al. Partial Loss of TDP-43 Function Causes Phenotypes of Amyotrophic Lateral Sclerosis. Proc. Natl. Acad. Sci. 2014, 111 (12), E1121–E1129.